Struct Chem (2012) 23:551–580
DOI 10.1007/s11224-011-9895-8

ORIGINAL RESEARCH

Quantum investigation of non-bonded interaction between the $B_{15}N_{15}$ ring and BH_2NBH_2 (radical, cation, anion) systems: a nano molecularmotor

Majid Monajjemi

Received: 14 July 2011 / Accepted: 9 October 2011 / Published online: 1 November 2011

Abstract The electromagnetic non-bonded interactions of BH_2NBH_2 molecule inside the $B_{15}N_{15}$ ring has been investigated with B3LYP method using EPR-II and EPR-III basis sets. Optimized structures, relative stability, and hyperfine spectroscopic parameters, such as total atomic charges, spin densities, electrical potential, and isotropic Fermi coupling constants of radical, cationic, and anionic forms of BH_2NBH_2 in different loops and bonds have been calculated. The spectral properties have been contributed to explain the characteristics of hyperfine electronic structure. The calculation for the $B_{15}N_{15}$–BH_2NBH_2 system and then for adenine–thymine base pairs coupled with BH_2NBH_2 molecule inside the $B_{15}N_{15}$ ring (A–BNB–T) have been done and three quantized rotational frequencies for transitions among cationic, radical, and anionic have been calculated, too. All observed frequencies appeared in the IR rotational region. So, this system can be used for the measurement of rotational spectra related to electrical voltage differences existing in macromolecules such as proteins and DNA and membrane. Extensive calculations have been carried out on the radical, anionic, and cationic forms of BH_2NBH_2 to obtain data and it has been observed that the radial coordinate of the dipole moment vector (r) as well as the voltage differences (ΔV) and relative energies (ΔE) exhibited Gaussian distribution. We have obtained a relationship between dipole moments and the voltage differences and energies of system.

M. Monajjemi (✉)
Department of Chemistry, Science and Research Branch, Islamic Azad University, Tehran, Iran
e-mail: m_monajjemi@yahoo.com

Keywords Boron nitride cages · Non-bounded interaction · NQR · HOMO · LUMO · NBO · Hyperfine properties · DFT · Dipole moment · EPR-II · EPR-III

Introduction

Due to excellent thermal and chemical stability, boron nitride ceramics are traditionally used as parts of high-temperature equipment. Boron nitride has a great potential in nanotechnology. The thermal conductivity of BN is among the highest of all electric insulators. Little is known on the electronic structure and electromagnetic behavior of boron nitride in non-bonded interactions. Boron nitride has an isoelectric feature and exists in various crystalline forms, including hexagonal and cubic forms. The hexagonal form corresponding to graphite is the most stable and softest one and is employed as the lubricant and an additive to cosmetic products. The cubic form of BH_2NBH_2 analogous to diamond is called cubic BN. The initial BH_2NBH_2 form is amorphous BN powder and layers of amorphous boron nitride have application in some semiconductor devices. As diamond is less stable than graphite, cubic BN is less stable than hexagonal BN. The wurtzite form of BN is a hexagonal polymorph of carbon. In both cubic and wurtzite BN, boron and nitrogen atoms are classified as tetrahedral, but the angles between neighboring tetrahedral are different [1–4]. The both hexagonal and cubic BN are wide-gap semiconductors with a band gap energy corresponding to the UV region. If voltage is applied to hexagonal BN or cubic BN, it emits UV light in the range 215–250 nm and can be employed as a light emitting diode or laser [5, 6]. The physical properties and structural features of amorphous and crystalline BN, graphite and diamond are as follows [1–6]:

Material	Amorphous BN	Hexagonal-BN	Cubic BN	Wurtzite BN	Graphite	Diamond
Density (g/cm^3)	2.28	2.1	3.45	3.49	2.1	3.515
Mohs hardness	–	1–2	10	10	1–2	10
Knoop hardness (GPa)	10	–	45	34	–	100
Bulk modulus (GPa)	100	36.5	400	400	34	440
Thermal conductivity (W/cm K)	0.03	6	7.4	–	2–20	6–20
Thermal expansion (10^{-6}/ °C)	–	−2.7	1.2	2.7	−1.5	0.8
Bandgap (ev)	5.05	5.2	6.4	4.5–5.5	0	5.5
Refractive index	1.7	1.8	2.1	2.05	–	2.4
Magnetic susceptibility (μemu/g)	–	−0.48	–	–	−0.2	−1.6

Due to isoelectric characteristic of the non-carbon species $(BN)_n$ these compounds can be considered as a limiting case of the B/N doped fullerenes and have become a subject of research interest. This interest may be linked to the fact that boron nitride has a stable crystalline phase similar to graphite [10–12]. The synthesis of C_{60} fullerene [13] followed by that of larger fullerenes and carbon nanotubes raised the curtain on a new class of nano-objects based on layered materials with predicted unique intrinsic physical properties [14]. The production of these novel graphite-like nanostructures opens up a new era in materials science and nano-scale engineering [15].

There has been a significant interest in experimental studies of B_nN_m clusters that can be found in the literature, and several research groups have described the production of boron nitride-based nano-structures [16–21]. Recently, various cages and $(BN)_n$ cubes have been synthesized [22–27], BN polyhedral have also been successfully synthesized by reaction of BCl_3 with NH_3 in a laser beam [28, 29]. There are mainly two structural classes for $(BN)_n$ cages [25, 30]. One is constructed from alternate BN units and governed by an isolated square rule [19, 31], which is the counterpart of the isolated pentagon rule [32] of carbon fullerenes. Another class is of fullerene-like structures, based on combination of 5- and 6-membered rings, with the existence of N–N and B–B bonds. In addition to the theoretical predictions for the structures, physical properties of such molecules of $B_{24}C_{12}N_{24}$ molecule [30] and the $B_{12}N_{12}$, $B_{16}N_{16}$ and $B_{28}N_{28}$ molecules, the experimental synthesis and various spectrometer are needed for the final confirmation of their stability for structures [19, 33]. However, there is basically no experimental information on the B_nN_m cluster thermochemistry, though some information for small aggregates can be derived from ab initio calculations [34–37].

In view of the structural similarity of graphite and bulk boron nitride, it is usual to discuss these new materials in terms of modifications of the carbon fullerene and nanotube models.

A boron nitride nanotube can be imagined as a graphite-like sheet rolled on itself, where carbon atoms are alternately substituted by nitrogen and boron atoms. Structurally, it is a close analog of the carbon nanotube, namely a long cylinder with diameter of several to hundred nanometers and length of many microns. Nanotubes of BN have a structure similar to that of carbon nanotubes, i.e., graphene (or BN) sheets rolled on themselves where as carbon nanotubes can be metallic or semi-conducting depending on the rolling direction and radius, a BN nanotube is an electrical insulator with a wide band gap of 5.5 eV which is almost independent of tube chirality and morphology. It has a layered structure similar to graphite. In each layer, boron and nitrogen atoms are bound by strong covalent bonds, whereas layers are held together by weak van der Waals forces [7–9].

We have employed single wall borane nanotube (SWBNNT) from kind MWNT = 1, as an armchair nanotubes (n, m) with chirality $n = 5, m = 5$ and the tube length was 3 Å. The schematics of the generation of our considered nanotube through folding a section of a graphene sheet and the optimized structure of adenine–$B_{15}N_{15}$–thymine are displayed in the scheme, where $C = n\,a_1 + m\,a_2 = (n, m)$, a_1 and a_2 are the primitive lattice vectors of the graphene, and n, m are integers (Scheme 1) [38, 39].

The major focus of the present study was the investigation of the electrostatic interactions within the BNB–$B_{15}N_{15}$ system. For further investigation about electrostatic interactions, the quantum mechanical atomic charges caused by the asymmetric distribution of electrons in chemical bonds play an important role in simulations of intermolecular forces and condensed phase properties and they are also often used for a qualitative understanding of the structural aspects and mutual electrostatic interaction of two molecules [40]. Recently, an increasing number of studies on atomic charges have been performed [41–44]. Moreover, nuclear quadrupole resonance (NQR) parameters have been known as the proper tool for the description of the electrostatic interaction and charge transfer properties of $B_{15}N_{15}$–BNB system

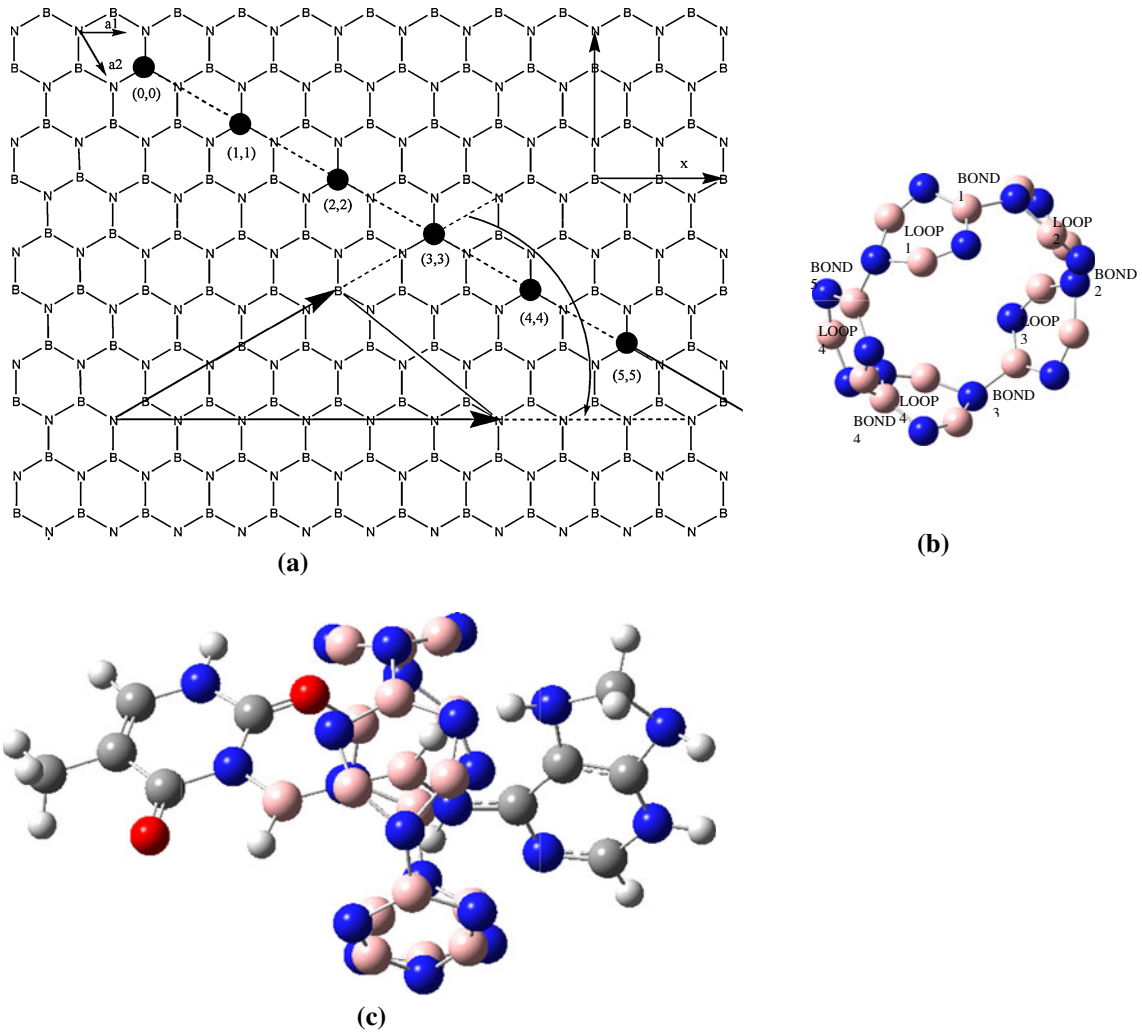

Scheme 1 **a** The geometrical structure of the generation of the armchair nanotube ($n = m = 5$) through folding a section of a graphene sheet. **b** The optimized structure of $B_{15}N_{15}$ ring at the level of B3LYP/EPR-III theory. **c** The optimized structure of adenine–$B_{15}N_{15}$–thymine at the level of B3LYP/EPR-III theory

[45–47]. In this study, to accomplish the evaluation of partial atomic charges we have used chelp G quantum chemical ECP method for various anion, cation, and radical types of BNB molecule inside the $B_{15}N_{15}$ ring.

The main objective of this study was to gain further insight into the electrostatic as well as electromagnetic nature of these non-bonded interactions in accounting for the capability of quantized rotation of BNB molecule inside the $B_{15}N_{15}$ ring. The character of interactions has been compared along with translation and rotation of radical, cationic, and anionic forms of BNB in $B_{15}N_{15}$–BNB system through calculations of the following different physicochemical parameters.

The main goal was to make a systematic exploration of the structure pattern of these boron nitrogen cage structures, i.e., presuming the $B_{15}N_{15}$ ring as a quantum mechanical rotating system holding a specific rotation axis as BNB, we planned to simulate BNB inside the $B_{15}N_{15}$ ring in accordance with an quantized nano-spectrophotometer detection of various quantized parameters of a given biomolecule.

Indeed, a comprehensive picture of the electronic structure of these magnetically unusual nano-particles motivated us to imagine such a nano-system as like as a quantized mechanic rotating system which would induced an electromagnetic field through electrostatic interaction of BNB to the $B_{15}N_{15}$ ring and also has a capability of detecting the quantized parameters of the system considered as well as other bimolecular systems which can be coupled with this system. In other words; there is mutual electrostatic interaction between BNB and the $B_{15}N_{15}$ ring which causes the quantization of the radial component of the dipole moment vector (r) as well as the voltage differences (ΔV) and relative energies (ΔE) of BNB radical,

cation, and anion. The BNB molecule rotate among quantized rotational levels of the radial component (r) of the dipole moment as well as energy levels and then specific spectrum would be appeared. We will explain in the next pages how this system can be used as a detector for biological molecules. In other words, when BNB is coupled with two points of the $B_{15}N_{15}$ ring. Different radical, cationic, and anionic forms of BNB are expected to appear because of the potential energy difference or voltage caused by the BNB. So, investigation of the electrostatic interaction of BNB with its surrounding ring evaluating variations of different physicochemical properties such as dipole and quadrupole moments as well as natural bond orbital (NBO) and NQR parameters of the BH_2NBH_2–$B_{15}N_{15}$ system is of great interest.

For instance, adenine–thymine base pairs have been coupled with BNB molecule inside the $B_{15}N_{15}$ ring and the same calculations repeated for the three different radical, anionic, and cationic forms of BNB. It is notable that for each case specific quantized values of the dipole moment (the radial component) and values have been obtained and all these quantized values satisfied with Gaussian distributions and different expectation values $\langle \Delta E \rangle$, $\langle \Delta V \rangle$, and $\langle \Delta r \rangle$ that can be referred to each quantized level. In this Gaussian curve, the system could undergo transitions among different quantized levels and yield a spectrum with three rotational frequencies ($\nu_{\text{radical–cation}}$, $\nu_{\text{anion–cation}}$, and $\nu_{\text{radical–anion}}$) while it returns to its ground state. Hence, based on the coupled biomolecules a unique spectrum of quantized parameters is distinguishable and this system can act like a biological nano spectrophotometer.

We anticipate that examining such an imagined prediction would be a promising way to improve the physical and chemical properties of fullerenes and may serve as a starting point for designing and considering electromagnetic nano systems in experiments.

To establish this target, it seems to be of importance to examine the structural stability of the BNB–$B_{15}N_{15}$ system. It is expected that BNB will be located strictly inside the $B_{15}N_{15}$ ring. So, the BNB–$B_{15}N_{15}$ system has been optimized using hybrid DFT calculations at the B3LYP level of theory as an efficient tool for theoretical studies on $(BN)_n$ rings and cages [22, 23] with the EPR-II and EPR-III proposed by Barone [13] as suitable basis sets for identification of the electromagnetic properties of nano-systems.

In order to test the radical, cationic, and anionic forms of the system's stability [48, 49], we have calculated the barrier energies as well as BSSE values in transitions and rotation of BNB at specific distances and rotational angles and also in each case the structural stability as well as conductivity of the system through calculating the highest occupied molecular orbital (HOMO)–lowest unoccupied molecular orbital (LUMO) band gap. In addition, analysis of the total atomic charges, electron spin density, and isotropic fermi coupling constants provided valuable information on the interaction characteristics. The NBO analysis has also been investigated to study the intermolecular orbital interactions in the complexes [50–53].

Computational details

The geometry of the $B_{15}N_{15}$ ring and BNB have been optimized by Becke's hybrid three-parameter exchange functional and the non-local correlation functional of Lee, Yang, and Parr (B3LYP) method [54, 55] with EPR-II and EPR-III basis sets of Barone [13] using ab initio GAUSSIAN quantum chemical package [56]. EPR-II is a double zeta basis set with a single set of polarization functions and an enhanced s-part: (6,1) [13, 23] for H and (10,5,1) [13, 14, 25] for B–F. EPR-III is a triple-zeta basis set including diffuse functions, double d-polarizations, and a single set of f-polarization functions. Also, in this case the s-part is improved to better describe the nuclear region: (6,2) [11, 14] for H and [13, 14, 26, 29] for B–F. Vibrational frequencies have been calculated at the level of B3LYP/EPR-II theory to verify that the geometry was a real minimum without any imaginary frequency and analyze the thermochemical functions including enthalpies and Gibbs free energies [57].

Standard quantum chemical calculations usually give exaggerated values of the binding energies of weakly bonded complexes. The BSSE is a consequence of the finite basis set approximation used in the calculations. The description of the intra-molecular energy of both individual molecules, namely BNB and the $B_{15}N_{15}$ ring is wanted within the nano system as compared with the calculations performed for the free separate molecules. Since the basis orbitals of the partner molecule are also available, the most commonly used cure for BSSE is to perform "counter poise" CP corrections defined by Boys and Bernar [58–60]. In this approach, we can determine the interaction energy by computing the energy of the free BNB and $B_{15}N_{15}$ individually for every geometrical arrangement of the system. So, in this study the BSSE corrections were applied during the optimizations and the interaction energies were evaluated.

In addition, we have obtained dipole moments as the coefficients of a series expansion of a potential because of continuous or discrete sources such as an electric charge distribution. If we consider a molecule consisting of N particles with charges eZ_i, the particle i has spherical polar coordinates r_i, θ_i, and φ_i. The electrostatic dipole operator is:

$$Q_l^j = \sum_{i=1}^{N} eZ_i R_l^m(r_i) \tag{1}$$

where, $R_l^m(r_i)$ is a regular solid harmonic function [61–63].

Moreover, the Breneman and Wiberg [64] approach based on the atomic charges derived from electrostatic potentials has been examined using a grid based method to quantitatively estimate the electrostatic interaction between BNB and $B_{15}N_{15}$ ring.

The NBO analysis has also been applied to study the intermolecular orbital interactions in the complexes [65, 66]. Also, the isotropic Fermi [67] coupling which depends on the direct transfer of electron spin to the s orbital of a proton, total atomic charges, spin densities, and electric potential of cationic and anionic forms of BNB in different loops and bonds of $B_{15}N_{15}$–BNB system have been evaluated with EPR-II and EPR-III basis sets to get a deeper insight about the non-bonded electrostatic interaction between BNB and the $B_{15}N_{15}$ ring.

Results and discussion

The aim of this section is to first discuss the different aspects of electronic structure of the BNB–$B_{15}N_{15}$ system for further validation of the theoretical results to increase their usefulness in practical applications or for pre-experimental modeling. Second, we have explored the electromagnetic nature of BNB inside the $B_{15}N_{15}$ ring through calculating the following parameters which provide valuable information on the interaction characteristics.

In this regard, the DFT method [68, 69] that includes electron correlation effects with the EPR-II and EPR-III basis sets of Barone [13] made it possible to analyze the electromagnetic behavior of the BNB–$B_{15}N_{15}$ system [70]. The EPR-III has been distinguished as a suitable basis set for description of hyperfine properties of the system considered. However, because of the time-consuming factor of EPR-III calculations, the EPR-II basis set has also been used to provide logical results.

Structural aspects of the BNB–$B_{15}N_{15}$ system

According to our best knowledge, detailed structural analysis in the forms of bond lengths and angles are still infrequent in theoretical studies on $(BN)_n$ rings. On the other hand, the oligomers and solids of $(BN)_n$ cages have attracted the interest of theorists [27]. Throughout this article, bond lengths are given in angstrom, bond angles in degrees and their corresponding geometries of the isolated $B_{15}N_{15}$ ring and BNB molecule have been compared before and after optimization. The variation of bond lengths (A°) and bond angles in the $B_{15}N_{15}$ ring and BNB–$B_{15}N_{15}$ systems are discussed. Compared with the pure $B_{15}N_{15}$ ring structure, it can be seen that the lengths of bonds which connect the loops have been decreased and the B–N–B bond angles have been increased. However, it is interesting that through inserting BNB inside one $B_{15}N_{15}$ ring, the electrostatic non-bonding interaction between BNB and $B_{15}N_{15}$ caused the increase of connecting B–N bonds from 1.496 up to 1.499 Å as well as increase of the B–N–B bond angels from 121.183 up to 121.721 Å.

The relative energies

To verify the structural stability of our considered BNB–$B_{15}N_{15}$ system, we have optimized the geometry of the BH_2NBH_2–$B_{15}N_{15}$ system using the B3LYP method with both EPR-II and EPR-III basis sets. The calculated energy (Hartree), relative energy (kcal/mol), and BSSE (kcal/mol) corrected interaction energy (kcal/mol) for cationic and anionic forms of BNB in the $B_{15}N_{15}$–BH_2NBH_2 system with transition and rotation are compared in Table 1.

Strikingly, despite the intrinsic linearity of BH_2NBH_2 in different radical, cationic, and anionic forms, the distortion of the BNB molecule occurs. The optimized results obtained confirm the stability the $B_{15}N_{15}$–BH_2NBH_2 system and the BNB molecule is located strictly in the middle of the $B_{15}N_{15}$ ring, vertically observed. According to the frequency calculation at the level of B3LYP/EPR-II theory, observing no negative frequency as well as obtaining thermochemical functions, such as $\Delta G = -749.679 \times 10^3$ kcal/mol, $\Delta H = -749.632 \times 10^3$ kcal/mol confirmed the structural stability of the $B_{15}N_{15}$ ring. This effect is probably because of the large dipole moments of the B–N bonds, which preferentially enhance the ring stability. Regarding stability of the system within transitions and rotations of radical, cationic, and anionic forms of BNB, it is notable that the obtained barrier energy for radical was 5.159 kcal/mol and the barrier energies of cationic and anionic forms were close together (14.193 kcal/mol) which was not considerable. The graphs of rotational and transition energy barrier of radical, anionic, and cationic forms of BNB in $B_{15}N_{15}$–BH_2NBH_2 system has been displayed in Fig. 1. To account for these observations, two observed points is notable. First, for radical and cationic forms of BNB the most stable condition has been observed in the case that BNB located exactly in the middle of $B_{15}N_{15}$ ring, i.e., the coordination of nitrogen atoms were (0, 0, 0). However, for the cationic form of BNB this stability has been found were the coordination of nitrogen atoms were (0, 0, 0.2). Second, the reported BSSE data revealed that in spite of insignificant changes of barrier energies based on the plotted graphs, the whole trend have not changed essentially from those of the first energy calculations. These obtained results motivated us to investigate the rotation of BNB. So, we have rotated the BNB from up to 180° its center around one of its axis. In this case, the barrier energy

Table 1 The calculated energy (Hartree), relative energy (kcal/mol), BSSE (kcal/mol) corrected interaction energy (kcal/mol) for cationic and anionic forms of BNB in $B_{15}N_{15}$–BH_2NBH_2 system within transition and rotation

$(B_{15}$–$N_{15})$–BNB	Anion				Cation				Radical			
	ΔE (kcal/mol)		BSSE (kcal/mol)		ΔE (kcal/mol)		BSSE (kcal/mol)		ΔE (kcal/mol)		BSSE (kcal/mol)	
Transition (Å) Rotational angle	Transition	Rotation	Transition	Rotation	Transition	Rotation	Transition	Rotation	Transition	Rotation	Transition	Rotation
0.0 Å	6.532	–	6.614	–	0.0	–	0.0	–	1.380	–	1.248	–
−135.0°	–	0.0	–	0.0	–	0.0	–	0.0	–	0.0	–	0.0
0.2 Å	2.093	–	2.181	–	0.456	–	0.464	–	2.10	–	1.972	–
−115°	–	2.47	–	1.236	–	1.523	–	0.057	–	3.879	–	2.493
0.4 Å	4.151	–	4.256	–	1.767	–	1.795	–	2.924	–	2.816	–
−95.0°	–	8.12	–	6.858	–	−1.055	–	−2.561	–	12.031	–	10.605
0.6 Å	5.370	–	5.483	–	3.830	–	3.873	–	3.410	–	3.317	–
−75.0°	–	21.68	–	20.436	–	3.535	–	2.058	–	28.697	–	27.295
0.8 Å	6.620	–	6.713	–	5.668	–	5.701	–	4.276	–	4.171	–
−55.0°	–	31.91	–	30.758	–	11.339	–	9.936	–	41.773	–	40.462
1.0 Å	7.850	–	7.930	–	8.795	–	8.821	–	5.726	–	5.615	–
−35.0°	–	36.70	–	35.573	–	17.652	–	16.268	–	49.804	–	48.509
1.5 Å	13.473	–	13.399	–	14.038	–	14.193	–	6.759	–	6.702	–
−15.0°	–	26.38	–	25.128	–	10.894	–	9.399	–	42.056	–	40.641
2.0 Å	8.313	–	8.284	–	11.524	–	11.692	–	5.159	–	5.123	–
5.0°	–	12.88	–	11.686	–	0.626	–	−0.813	–	21.977	–	20.618
3.0 Å	2.636	–	2.616	–	2.257	–	2.460	–	2.267	–	2.258	–
25.°	–	6.23	–	4.977	–	−1.742	–	−3.223	–	8.631	–	7.225
3.5 Å	0.0	–	0.0	–	1.006	–	1.212	–	0.0	–	0.0	–
45.0°	–	3.12	–	1.912	–	0.517	–	−0.932	–	4.530	–	3.162

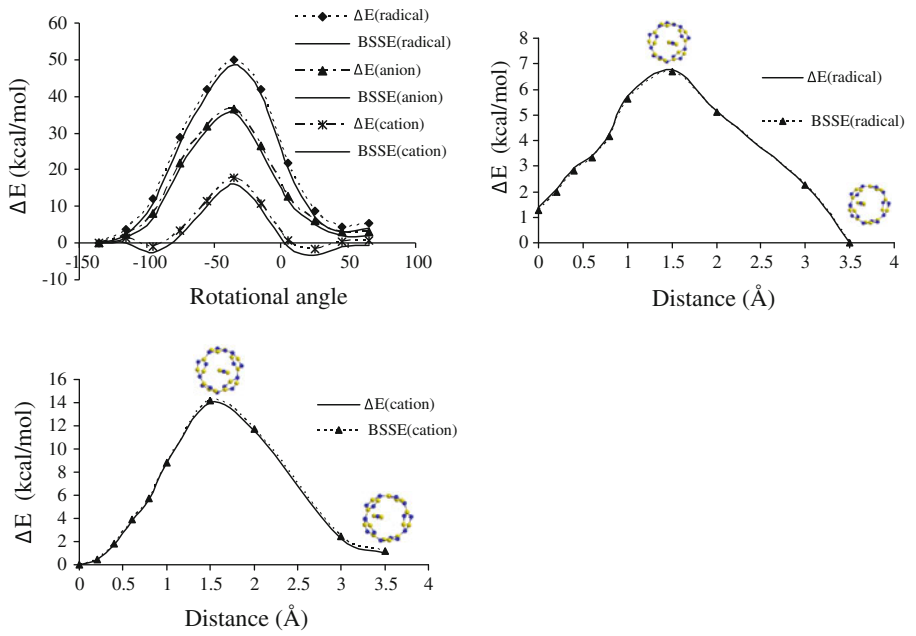

Fig. 1 Rotational and transition energy barriers of BNB in $B_{15}N_{15}$–BH_2NBH_2 system

was significant (49.804 kcal/mol). Based on such considerable high barrier energy we have observed that the BNB strongly resists under this rotation and exhibited no tendency for rotation in horizontal state.

It has been understood that the only possible movement which probably causes structural distortion of the system was internal rotation of BNB inside the ring (BE = 49.804 kcal/mol). It is evident that with such high barrier energy we could not expect any rotation.

According to the plotted rotational graph (Fig. 1), it has been found out that the energy barrier of BNB radical stands the highest value and the following trend could be observed:

$$\text{BNB (radical)} > \text{BNB (anion)} > \text{BNB (Cation)}$$

Based on the graph of rotational energy barrier of cationic form of BNB at different distances, it can be revealed that at $d = 1.5$ Å graph's pick has been observed, as the barrier energy was 14.03814053 kcal/mol.

The HOMO–LUMO frontier orbitals

In order to check the validity of this description about the structural stability of the four species in the BNB–$B_{15}N_{15}$ system, the HOMO–LUMO frontier orbitals have been calculated. Recently, the HOMO–LUMO band gap has been suggested is a measure of the structural stability and semi-conducting properties of [71].

The band gap of the $B_{15}N_{15}$–BH_2NBH_2 system, the difference in energy of the HOMO and the LUMO in atomic unit is reported in Table 2. In particular, the HOMO, LUMO and the energy gaps E (LUMO)–E (HOMO) of the BNB anion stands out as the largest in the states considered. Conversely, the lowest HOMO–LUMO band gaps correspond to both rotation and transition of the BNB cation and were in the range of 0.03364–0.08695 atomic unit which showed the lowest stability and highest conductivity of this form.

As a whole, the band gap for all three radical, anion, and cation forms of BNB were as follows:

$$\text{BH}_2\text{NBH}_2\,(\text{anion}) > \text{BH}_2\text{NBH}_2\,(\text{radical}) > \text{BH}_2\text{NBH}_2\,(\text{Cation})$$

Therefore, it can be concluded that for both transition and rotation the most stability and less conductivity can be expected for the BNB anion. In addition, for the case of both anion and radical BNB the highest band gap and the highest stability have been observed in the same distance at 1 Å, which were 26.97219 and 26.70761 a.u. at 1.5 Å, respectively. Also, for both cation and anion BNB the highest band gap and then the highest stability have been found at −35°. However, for the case of radical rotation of BNB the highest stability has been found at −135°.

It is interesting that if we just consider the HOMO–LUMO band gap of the $B_{15}N_{15}$ ring that has a small band gap (0.17908 a.u.), it can be concluded that the existence of BNB inside the $B_{15}N_{15}$ ring and its electrostatic interaction for both anionic and radical forms caused the higher conductivity compared with the pure ring and because of feasibility of electron transfer it is expected that in these anionic and radical cases the electromagnetic induction would be improved.

Table 2 The band gap of $B_{15}N_{15}$–BH_2NBH_2 system as the relative differences in the energy of the HOMO and the LUMO in atomic unit

Anion				Cation				Radical			
Transition		Rotation		Transition		Rotation		Transition		Rotation	
d (Å)	Band gap (HOMO–LUMO)	Angle	Band gap (HOMO–LUMO)	*d* (Å)	Band gap (HOMO–LUMO)	Angle	Band gap (HOMO–LUMO)	*d* (Å)	Band gap (HOMO–LUMO)	Angle	Band gap (HOMO–LUMO)
0.0	26.94872	−135.0	26.93602	0.0	0.04097	−135.0	0.04099	0.0	–	−135.0	26.70356
0.2	26.93661	−115.0	26.94033	0.2	0.04136	−115.0	0.04554	0.2	26.70317	−115.0	26.69834
0.4	26.93366	−95.0	26.94441	0.4	0.03878	−95.0	0.05605	0.4	26.70195	−95.0	26.6954
0.6	26.93289	−75.0	26.95322	0.6	0.03739	−75.0	0.07206	0.6	26.70133	−75.0	26.68908
0.8	26.93626	−55.0	26.9631	0.8	0.0359	−55.0	0.08142	0.8	26.70341	−55.0	26.68162
1.0	26.93717	−35.0	26.97219	1.0	0.03469	−35.0	0.08695	1.0	26.70703	−35.0	26.68881
1.5	26.96448	−15.0	26.95524	1.5	0.03307	−15.0	0.08537	1.5	26.70761	−15.0	26.67217
2.0	26.94224	5.0	26.95442	2.0	0.03364	5.0	0.06848	2.0	26.68134	5.0	26.68588
3.0	26.91099	25.0	26.94304	3.0	0.03497	25.0	0.05448	3.0	26.64713	25.0	26.69781
3.5	26.90572	45.0	26.94453	3.5	0.03459	45.0	0.04674	3.5	26.65182	45.0	26.69803
Ring (EPR-II)	0.17908	65.0	26.94217	–		65.0	0.04866	–		65.0	26.69464

NBO analysis

In the NBO analysis, the interaction arising from electron delocalization are analyzed by selecting a number of natural bonding and anti-bonding orbitals that distort from the idealized Lewis structure, caused by interactions among them through hyper-conjugative or electrostatic interactions. In NBO analysis, the input atomic orbital basis set is transformed via natural atomic orbitals (NAOs) and natural hybrid orbital (NHOs) into NBO [72–74].

In the present theoretical study, particular attention has been paid to the structural properties of our BNB–$B_{15}N_{15}$ system. So, the NBO analysis gives supplementary information of the relative structural properties [57]. It should be noted that conjugated systems, such as benzene and π-conjugated linear molecules, have been well studied with NBO analysis [75–77].

NBO analysis of the $B_{15}N_{15}$–BNB system at the level of B3LYP/EPR-II theory considering radical, cationic, and anionic forms of BNB with different rotational angles has been given in Table 3. The coefficients of *s* and *p* orbitals of both B–N and B–B bonds involved in radical, cation, and anion $B_{15}N_{15}$–BNB as well as the hybridization of B and N atoms can be distinguished based on these NBO data.

It has been found that at all rotational angles the bonding and anti-bonding coefficients of *s* and *p* orbitals of N–B bonds were 0.4 and 0.9. However, for the B–B bonds the constant coefficient (0.7) was obvious. Based on the constant values of the coefficients of linear combination of s and p orbitals of different bonds (0.4 and 0.9), a specific voltage differences could be expected.

It is notable that the percent of *s* and *p* orbital's of different bonds of BNB anion in BNB–$B_{15}N_{15}$ system at all rotational angles corresponds sp^2 hybridization which is in good agreement with the intrinsic sp^2 hybridization of the B atom. Hence, it can be concluded that the most structural stability is expected for BNB anion in BH_2NBH_2 system at all rotational angles.

Another logical relationship could be found between NBO and ΔV values of different bonds of $B_{15}N_{15}$–BNB system. To compare in more details, it can be concluded that in the case of BNB anion the closeness of obtained the ΔV values (20.642–21.758 a.u.) derived by EPR calculations were in accordance with the estimation of the sp^2 hybridization of B atom derived by NBO analysis, while such a direct relationship has not been observed for the BNB cation case. In other words, via a comparison of average value of ΔV in the case of BNB anion the low average ($\Delta V = 21.171$ a.u.) revealed the sharp Gaussian distribution and could be related with the constant bonding molecular orbital coefficients. Meanwhile, the opposite behavior has been seen for the BNB cation.

NQR parameters

NQR has proven to be a sensitive technique for the study of hyperfine structure and dynamics in nano-systems and will assist in the future assignment of such spectral data [45–47].

The NQR parameters of nitrogen atoms of $B_{15}N_{15}$ from the B3LYP method using EPR-II and EPR-III basis sets are listed in Table 4. The quadrupole coupling constant (χ) as well as the asymmetry parameter (η) of the electric field gradient (EFG) tensor of nitrogen atoms of the $B_{15}N_{15}$ ring are related to the electric charge distribution within the molecule as well as to the intra-molecular interactions.

Table 3 NBO analysis of the $B_{15}N_{15}$–BH_2NBH_2 system considering radical, cationic, and anionic forms of BNB with different rotational angles at the level of B3LYP/EPR-II theory

Rotational angle	Bond	NBO analysis		
		Anion	Cation	Radical
−135.0	BD (1) N31–B32	$0.9010*(sp^{1.00})N + 0.4338*(sp^{2.67})B$	$0.9016*(sp^{1.00})N + 0.4325*(sp^{1.19})B$	$0.9070*(sp^{1.00})N + 0.4210*(sp^{3.06})B$
	BD (2) N31–B32	–	–	$0.9469*(p^{1.00})N + 0.3216*(p^{1.00}d^{0.01})B$
	BD (1) N31–B33	$0.9010*(sp^{1.00})N + 0.4338*(sp^{2.67})B$	$0.9016*(sp^{1.00}) + 0.4325*(sp^{1.19})B$	$0.9070*(sp^{1.00})N + 0.4211*(sp^{3.06})B$
	BD (2) N31–B33	–	$0.9493*(p^{1.00})N + 0.3143*(p^{1.00}d^{0.01})B$	–
	BD*(1) B32–B33	$0.7072*(p^{1.00})B - 0.7070*(p^{1.00})B$	$0.7071*(sp^{0.83})B - 0.7071*(sp^{0.83})B$	–
	BD*(1) N31–B32	$0.4338*(sp^{1.00})N - 0.9010*(sp^{2.67})B$	$0.4325*(sp^{1.00})N - 0.9016*(sp^{1.19})B$	$0.4210*(sp^{1.00})N - 0.9070*(sp^{3.06})B$
	BD*(2) N31–B32	–	–	$0.3216*(p^{1.00})N - 0.9469*(p^{1.00})B$
	BD*(1) N31–B33	$0.4338*(sp^{1.00})N - 0.9010*(sp^{2.67})B$	$0.4325*(sp^{1.00})N - 0.9016*(sp^{1.19})B$	$0.4211*(sp^{1.00})N - 0.9070*(sp^{3.06})B$
	BD*(2) N31–B33	–	$0.3143*(p^{1.00})N - 0.9493*(p^{1.00}d^{0.01})B$	–
	BD (1) B32–B33	$0.7070*(p^{1.00})B + 0.7072*(p^{1.00})B$	$0.7071*(sp^{0.83})B + 0.7071*(sp^{0.83})B$	–
−115.0	BD (1) N31–B32	$0.9012*(sp^{1.00})N + 0.4334*(sp^{2.69})B$	$0.9017*(sp^{1.00})N + 0.4323*(sp^{1.18})B$	$0.9073*(sp^{1.00})N + 0.4205(sp^{3.09})B$
	BD (2) N31–B32	–	–	$0.9471*(p^{1.00})N + 0.3208*(sp^{1.00}d^{0.01})B$
	BD (1) N31–B33	$0.9011*(sp^{1.00})N + 0.4336*(sp^{2.68})B$	$0.9017*(sp^{1.00})N + 0.4324*(sp^{1.18})B$	$0.9072*(sp^{1.00})N + 0.4207*(sp^{3.07})B$
	BD (2) N31–B33	–	$0.9493*(p^{1.00})N + 0.3144*(p^{1.00}d^{0.01})B$	–
	BD*(1) B32–B33	$0.7084*(p^{1.00})N - 0.7058*(p^{1.00})B$	$0.7076*(sp^{0.83})B - 0.7066*(sp^{0.83})B$	–
	BD*(1) N31–B32	$0.4334*(sp^{1.00})N - 0.9012*(sp^{2.69})B$	$0.4323*(sp^{1.00})N - 0.9017*(sp^{1.18})B$	$0.4205*(sp^{1.00})N - 0.9073*(sp^{3.09})B$
	BD*(2) N31–B32	–	–	$0.3208*(p^{1.00})N - 0.9471*(p^{1.00}d^{0.01})B$
	BD*(1) N31–B33	$0.4336*(sp^{1.00})N - 0.9011*(sp^{2.68})B$	$0.4324*(sp^{1.00})N - 0.9017*(sp^{1.18})B$	$0.4207*(sp^{1.00})N - 0.9072*(sp^{3.07})B$
	BD*(2) N31–B33	–	$0.3144*(p^{1.00})N - 0.9493*(p^{1.00}d^{0.01})B$	–
	BD (1) B32–B33	$0.7058*(p^{1.00})B + 0.7084*(p^{1.00})B$	$0.7066*(sp^{0.83})B + 0.7076*(sp^{0.83})B$	–
−95.0	BD (1) N31–B32	$0.9012*(sp^{1.00})N + 0.4334*(sp^{2.69})B$	$0.9017*(sp^{1.00}N + 0.4324*(sp^{1.18})B$	$0.9073*(sp^{1.00})N + 0.4205*(sp^{3.09})B$
	BD (2) N31–B32	–	–	$0.9471*(p^{1.00})N + 0.3209*(p^{1.00}d^{0.01})B$
	BD (1) N31–B33	$0.9011*(sp^{1.00})N + 0.4335*(sp^{2.68})B$	$0.9017*(sp^{1.00})N + 0.4324*(sp^{1.18})B$	$0.9072*(sp^{1.00})N + 0.4207*(sp^{3.07})B$
	BD (2) N31–B33	–	$0.9493*(p^{1.00})N + 0.3143*(p^{1.00}d^{0.01})B$	–
	BD*(1) B32–B33	$0.7083*(p^{1.00})B - 0.7059*(p^{1.00})B$	$0.7076*(sp^{0.83})B - 0.7066*(sp^{0.83})B$	–
	BD*(1) N31–B32	$0.4334*(sp^{1.00})N - 0.9012*(sp^{2.69})B$	$0.4324*(sp^{1.00})N - 0.9017*(sp^{1.18})B$	$0.4205*(sp^{1.00})N - 0.9073*(sp^{3.09})B$
	BD*(2) N31–B32	–	–	$0.3209*(p^{1.00})N - 0.9471*(p^{1.00}d^{0.01})B$
	BD*(1) N31–B33	$0.4335*(sp^{1.00})N - 0.9011*(sp^{2.68})B$	$0.4324*(sp^{1.00})N - 0.9017*(sp^{1.18})B$	$0.4207*(sp^{1.00})N - 0.9072*(sp^{3.07})B$
	BD*(2) N31–B33	–	$0.3143*(p^{1.00})N - 0.9493*(p^{1.00}d^{0.01})B$	–
	BD (1) B32–B33	$0.7059*(p^{1.00})B + 0.7083*(p^{1.00})B$	$0.7066*(sp^{0.83})B + 0.7076*(sp^{0.83})B$	–

Table 3 continued

Rotational angle	Bond	NBO analysis		
		Anion	Cation	Radical
−75.0	BD (1) N31–B32	$0.9012*(sp^{1.00})N + 0.4334*(sp^{2.69})B$	$0.9017*(sp^{1.00})N + 0.4323*(sp^{1.18})B$	$0.9073*(sp^{1.00})N + 0.4205*(sp^{3.09})B$
	BD (2) N31–B32	–	–	$0.9471*(p^{1.00})N + 0.3209*(p^{1.00}d^{0.01})B$
	BD (1) N31–B33	$0.9011*(sp^{1.00})N + 0.4335*(sp^{2.68})B$	$0.9017*(sp^{1.00})N + 0.4324*(sp^{1.18})B$	$0.9072*(sp^{1.00})N + 0.4207*(sp^{3.07})B$
	BD (2) N31–B33	–	$0.9493*(p^{1.00})N + 0.3143*(p^{1.00}d^{0.01})B$	–
	BD*(1) B32–B33	$0.7054*(p^{1.00})N - 0.7058*(p^{1.00})B$	$0.7076*(sp^{0.83})B - 0.7066*(sp^{0.83})B$	–
	BD*(1) N31–B32	$0.4334*(sp^{1.00})N - 0.9012*(sp^{2.69})B$	$0.4323*(sp^{1.00})N - 0.9017*(sp^{1.18})B$	$0.4205*(sp^{1.00})N - 0.9073*(sp^{3.09})B$
	BD*(2) N31–B32	–	–	$0.3209*(p^{1.00})N - 0.9471*(p^{1.00}d^{0.01})B$
	BD*(1) N31–B33	$0.4335*(sp^{1.00})N - 0.9011*(sp^{2.68})B$	$0.4324*(sp^{1.00})N - 0.9017*(sp^{1.18})B$	$0.4207*(sp^{1.00})N - 0.9072*(sp^{3.07})B$
	BD*(2) N31–B33	–	$0.3143*(p^{1.00})N - 0.9493*(p^{1.00}d^{0.01})B$	–
	BD (1) B32–B33	$0.7058*(p^{1.00})B + 0.7084*(p^{1.00})B$	$0.7066*(sp^{0.83})B + 0.7076*(sp^{0.83})B$	–
−55.0	BD (1) N31–B32	$0.9012*(sp^{1.00})N + 0.4334*(sp^{2.69})B$	$0.9017*(sp^{1.00})N + 0.4323*(sp^{1.18})B$	$0.9073*(sp^{1.00})N + 0.9073*(sp^{1.00})B$
	BD (2) N31–B32	–	–	$0.9471*(p^{1.00})N + 0.3209*(p^{1.00}d^{0.01})B$
	BD (1) N31–B33	$0.9011*(sp^{1.00})N + 0.4335*(sp^{2.68})B$	$0.9017*(sp^{1.00})N + 0.4324*(sp^{1.18})B$	$0.9072*(sp^{1.00})N + 0.4207*(sp^{3.07})B$
	BD (2) N31–B33	–	$0.9493*(p^{1.00})N + 0.3143*(p^{1.00}d^{0.01})B$	–
	BD*(1) B32–B33	$0.7082*(p^{1.00})N - 0.7060*(p^{1.00})B$	$0.7076*(sp^{0.83})B - 0.7066*(sp^{0.83})B$	–
	BD*(1) N31–B32	$0.4334*(sp^{1.00})N - 0.9012*(sp^{2.69})B$	$0.4323*(sp^{1.00})N - 0.9017*(sp^{1.18})B$	$0.4205*(sp^{1.00})N - 0.9073*(sp^{3.09})B$
	BD*(2) N31–B32	–	–	$0.3209*(p^{1.00})N - 0.9471*(p^{1.00}d^{0.01})B$
	BD*(1) N31–B33	$0.4335*(sp^{1.00})N - 0.9011*(sp^{2.68})B$	$0.4324*(sp^{1.00})N - 0.9017*(sp^{1.18})B$	$0.4207*(sp^{1.00})N - 0.9072*(sp^{3.07})B$
	BD*(2) N31–B33	–	$0.3143*(p^{1.00})N - 0.9493*(p^{1.00}d^{0.01})B$	–
	BD (1) B32–B33	$0.7060*(p^{1.00})B + 0.7082*(p^{1.00})B$	$0.7066*(sp^{0.83})B + 0.7076*(sp^{0.83})B$	–
−35.0	BD (1) N31–B32	$0.9012*(sp^{1.00})N + 0.4334*(sp^{2.69})B$	$0.9017*(sp^{1.00})N + 0.4323*(sp^{1.18})B$	$0.9073*(sp^{1.00})N + 0.4205*(sp^{3.09})B$
	BD (2) N31–B32	–	–	$0.9471*(p^{1.00})N + 0.3208*(p^{1.00}d^{0.01})B$
	BD (1) N31–B33	$0.9011*(sp^{1.00})N + 0.4335*(sp^{2.68})B$	$0.9017*(sp^{1.00})N + 0.4324*(sp^{1.18})B$	$0.9072*(sp^{1.00})N + 0.4207*(sp^{3.07})B$
	BD (2) N31–B33	–	$0.9493*(p^{1.00})N + 0.3143*(p^{1.00}d^{0.01})B$	–
	BD*(1) B32–B33	$0.7083*(sp^{1.00})B - 0.7059*(sp^{1.00})B$	$0.7076*(sp^{0.83})B - 0.7066*(sp^{0.83})B$	–
	BD*(1) N31–B32	$0.4334*(p^{1.00})N - 0.9012*(p^{2.69})B$	$0.4323*(sp^{1.00})N - 0.9017*(sp^{1.18})B$	$0.4205*(sp^{1.00})N - 0.9073*(sp^{3.09})B$
	BD*(2) N31–B32	–	–	$0.3208*(p^{1.00})N - 0.9471*(p^{1.00}d^{0.01})B$
	BD*(1) N31–B33	$0.4335*(sp^{1.00})N - 0.9011*(sp^{2.68})B$	$0.4324*(sp^{1.00})N - 0.9017*(sp^{1.18})B$	$0.4207*(sp^{1.00})N - 0.9072*(sp^{3.07}d^{0.02})B$
	BD*(2) N31–B33	–	$0.3143*(p^{1.00})N - 0.9493*(p^{1.00}d^{0.01})B$	–
	BD (1) B32–B33	$0.7059*(p^{1.00})B + 0.7083*(p^{1.00})B$	$0.7066*(sp^{0.83})B + 0.7076*(sp^{0.83})B$	–

Table 3 continued

Rotational angle	Bond	NBO analysis		
		Anion	Cation	Radical
−15.0	BD (1) N31–B32	$0.9012*(sp^{1.00})N + 0.4334*(sp^{2.68})B$	$0.9017*(sp^{1.00})N + 0.4324*(sp^{1.18})B$	$0.9073*(sp^{1.00})N + 0.4205*(sp^{3.09})B$
	BD (2) N31–B32	–	–	$0.9471*(p^{1.00})N + 0.3209*(p^{1.00}d^{0.01})B$
	BD (1) N31–B33	$0.9011*(sp^{1.00})N + 0.4335*(sp^{2.68})B$	$0.9017*(sp^{1.00})N + 0.4324*(sp^{1.18})B$	$0.9072*(sp^{1.00})N + 0.4207*(sp^{3.07})B$
	BD (2) N31–B33	–	$0.9493*(p^{1.00})N + 0.3143*(p^{1.00}d^{0.01})B$	–
	BD*(1) B32–B33	$0.7086*(p^{1.00})B - 0.7056*(p^{1.00})B$	$0.7076*(sp^{0.83})B - .7066*(sp^{0.83})B$	–
	BD*(1) N31–B32	$0.4334*(sp^{1.00})N - 0.9012*(sp^{2.68})B$	$0.4324*(sp^{1.00})N - .9017*(sp^{1.18})B$	$0.4205*(sp^{1.00})N - 0.9073*(sp^{3.09})B$
	BD*(2) N31–B32	–	–	$0.3209*(p^{1.00})N - 0.9471*(p^{1.00}d^{0.01})B$
	BD*(1) N31–B33	$0.4335*(sp^{1.00})N - 0.9011*(sp^{2.68})B$	$0.4324*(sp^{1.00})N - 0.9017*(sp^{1.18})B$	$0.4207*(sp^{1.00})N - 0.9072*(sp^{3.07})B$
	BD*(2) N31–B33	–	$0.3143*(p^{1.00})N - 0.9493*(p^{1.00}d^{0.01})B$	–
	BD (1) B32–B33	$0.7056*(p^{1.00})B + 0.7086*(p^{1.00})B$	$0.7066*(sp^{0.83})B + 0.7076*(sp^{0.83})B$	–
5.0	BD (1) N31–B32	$0.9012*(sp^{1.00})N + 0.4334*(sp^{2.69})B$	$0.9017*(sp^{1.00})N + 0.4323*(sp^{1.18})B$	$0.9073*(sp^{1.00})N + 0.4205*(sp^{3.09})B$
	BD (2) N31–B32	–	–	$0.9471*(p^{1.00})N + 0.3208*(p^{1.00}d^{0.01})B$
	BD (1) N31–B33	$0.9011*(sp^{1.00})N + 0.4335*(sp^{2.68})B$	$0.9017*(sp^{1.00})N + 0.4324*(sp^{1.18})B$	$0.9072*(sp^{1.00})N + 0.4207*(sp^{3.07}B$
	BD (2) N31–B33	–	$0.9493*(p^{1.00})N + 0.3143*(p^{1.00}d^{0.01})B$	–
	BD*(1) B32–B33	$0.7082*(p^{1.00})N - 0.7060*(p^{1.00})B$	$0.7076*(sp^{0.83})B - 0.7066*(sp^{0.83})B$	–
	BD*(1) N31–B32	$0.4334*(sp^{1.00})N - 0.9012*(sp^{2.69})B$	$0.4323*(sp^{1.00})N - 0.9017*(sp^{1.18})B$	$0.4205*(sp^{1.00})N - 0.9073*(sp^{3.09})B$
	BD*(2) N31–B32	–	–	$0.3208*(p^{1.00})N - 0.9471*(p^{1.00}d^{0.01})B$
	BD*(1) N31–B33	$0.4335*(sp^{1.00})N - 0.9011*(sp^{2.68})$	$0.4324*(sp^{1.00})N - 0.9017*(sp^{1.18})B$	$0.4207*(sp^{1.00})N - 0.9072*(sp^{3.07})B$
	BD*(2) N31–B33	–	$0.3143*(p^{1.00})N - 0.9493*(p^{1.00}d^{0.01})B$	–
	BD (1) B32–B33	$0.7060*(p^{1.00})B + 0.7082*(p^{1.00})B$	$0.7066*(sp^{0.83})B + 0.7076*(sp^{0.83})B$	–
25.0	BD (1) N31–B32	$0.9012*(sp^{1.00})N + 0.4334*(sp^{2.69})B$	$0.9017*(sp^{1.00})N + 0.4324*(sp^{1.18})B$	$0.9073*(sp^{1.00})N + 0.4205*(sp^{3.09})B$
	BD (2) N31–B32	–	–	$0.9471*(p^{1.00})N + 0.3209*(p^{1.00}d^{0.01})B$
	BD (1) N31–B33	$0.9011*(sp^{1.00})N + 0.4335*(sp^{2.68})B$	$0.9017*(sp^{1.00})N + 0.4324*(sp^{1.18})B$	$0.9072*(sp^{1.00})N + 0.4207*(sp^{3.07})B$
	BD (2) N31–B33	–	$0.9493*(p^{1.00})N + 0.3143*(p^{1.00}d^{0.01})B$	–
	BD*(1) B32–B33	$0.7086*(p^{1.00})N - 0.7056*(p^{1.00})B$	$0.7076*(sp^{0.83})B - 0.7066*(sp^{0.83})B$	–
	BD*(1) N31–B32	$0.4334*(sp^{1.00})N - 0.9012*(sp^{2.69})B$	$0.4324*(sp^{1.00})N - 0.9017*(sp^{1.18})B$	$0.4205*(sp^{1.00})N - 0.9073*(sp^{3.09})B$
	BD*(2) N31–B32	–	–	$0.3209*(p^{1.00})N - 0.9471*(p^{1.00}d^{0.01})B$
	BD*(1) N31–B33	$0.4335*(sp^{1.00})N - 0.9011*(sp^{2.68})B$	$0.4324*(sp^{1.00})N - 0.9017*(sp^{1.18})B$	$0.4207*(sp^{1.00})N - 0.9072*(sp^{3.07})B$
	BD*(2) N31–B33	–	$0.3143*(p^{1.00})N - 0.9493*(p^{1.00}d^{0.01})B$	–
	BD (1) B32–B33	$0.7056*(p^{1.00})B + 0.7086*(p^{1.00})B$	$0.7066*(sp^{0.83})B + 0.7076*(sp^{0.83})B$	–

Table 3 continued

Rotational angle	Bond	NBO analysis		
		Anion	Cation	Radical
45.0	BD (1) N31–B32	$0.9012*(sp^{1.00})N + 0.4334*(sp^{2.69})B$	$0.9017*(sp^{1.00})N + 0.4324*(sp^{1.18})B$	$0.9073*(sp^{1.00})N + 0.4205*(sp^{3.09})B$
	BD (2) N31–B32	–	–	$0.9471(p^{1.00})N + 0.3209*(p^{1.00}d^{0.01})B$
	BD (1) N31–B33	$0.9011*(sp^{1.00})N + 0.4335*(sp^{2.68})B$	$0.9017*(sp^{1.00})N + 0.4324*(sp^{1.18})B$	$0.9072*(sp^{1.00})N + 0.4207*(sp^{3.07})B$
	BD (2) N31–B33	–	$0.9493*(p^{1.00})N + 0.3143*(p^{1.00}d^{0.01})B$	–
	BD*(1) B32–B33	$0.7085*(p^{1.00})N - 0.7057*(p^{1.00})B$	$0.7076*(sp^{0.83})B - 0.7066*(sp^{0.83})B$	–
	BD*(1) N31–B32	$0.4334*(sp^{1.00})N - 0.9012*(sp^{2.69})B$	$0.4324*(sp^{1.00})N - 0.9017*(sp^{1.18})B$	$0.4205*(sp^{1.00})N - 0.9073*(sp^{3.09})B$
	BD*(2) N31–B32	–	–	$0.3209*(p^{1.00})N - 0.9471*(p^{1.00}d^{0.01})B$
	BD*(1) N31–B33	$0.4335*(sp^{1.00})N - 0.9011*(sp^{2.68})B$	$0.4324*(sp^{1.00})N - 0.9017*(sp^{1.18})B$	$0.4207*(sp^{1.00})N - 0.9072*(sp^{3.07})B$
	BD*(2) N31–B33	–	$0.3143*(p^{1.00})N - 0.9493*(p^{1.00}d^{0.01})B$	–
	BD (1) B32–B33	$0.7057*(p^{1.00})B + 0.7085*(p^{1.00})B$	$0.7066*(sp^{0.83})B + 0.7076*(sp^{0.83})B$	–

According to the NQR parameters of nitrogen atoms which have been derived from the EFG tensor, two sets of nitrogen atom can be identified in the $B_{15}N_{15}$ ring structure. The first series had the lowest asymmetry parameters ($\eta = 0.1$). Meanwhile, the second group containing N_9, N_{15}, N_{22}, and N_{27} had high asymmetry parameters ($\eta = 0.5$), the lowest coupling constants (χ) and quadrupole frequencies (ν_+, ν_-). Moreover, a direct relationship can be seen between these NQR parameters and the EPR data reported in Tables 5 and 6. In other words, the more negative electrical potentials (−18) in both cation and radical forms corresponds to the nitrogen atoms with high asymmetry parameters. On the other band, especially in the case of the BNB anion these nitrogen atoms had the more negative atomic charges (−0.4 up to −0.07) derived by chelp G calculations. This relationship was more evident in the EPR-III results, i.e., the atomic charges of the second nitrogen group are more negative and for the BNB anion and radical were −0.8, −0.9, −0.4, and −0.7 a.u., respectively. Another observed point is that the lowest isotropic Fermi constants (IFC) have been obtained for this second group of nitrogen atoms. In the case of BNB anion this fact has been observed as yielding negative values of the IFC.

A comparison of the NQR parameters of nitrogen atoms with both EPR-II and EPR-III basis sets demonstrated that higher values of asymmetry parameters as well as the lower coupling constants (χ) and quadrupole frequencies (ν_+, ν_-) have been obtained with EPR-III basis set.

Electrostatic interaction of BNB with the $B_{15}N_{15}$ ring

In this section, the major point is the investigation of electrostatic interaction of BNB with its surrounding $B_{15}N_{15}$ ring which forms the basis for more detailed studies of other systems with non-bonded interaction. To investigate the electrostatic interaction on of BNB with five different segments including five loops and five connecting bonds of $B_{15}N_{15}$ ring within vertical transition, first the four pentagon loops have been frozen and the electrostatic interaction of BNB with the one remained active loop has been considered. Other loops have been examined one by one in the same way and the changes of all the following calculated quantities have been explored. Next, we were focused on each bond of $B_{15}N_{15}$ individually and evaluated the interaction of BNB with each of the five connecting bonds of $B_{15}N_{15}$ ring and repeated the calculations along each bond.

Analysis of dipole moments

The only known mechanisms for the creation of dipole moments are by current loops or quantum–mechanical spin since the existence of monopoles has never been experimentally demonstrated [78–80]. On the other hand, dipole

Table 4 NQR parameters of nitrogen atoms of $B_{15}N_{15}$ ring at the level of B3LYP/EPR-III theory

Atoms	η		χ (MHz)		$v+$ (MHz)		$v-$ (MHz)	
	EPR-II	EPR-III	EPR-II	EPR-III	EPR-II	EPR-III	EPR-II	EPR-III
N_2	0.4681	0.5284	2.0180	1.9001	1.7496	1.6760	1.2773	1.1740
N_3	0.2345	0.1234	2.3307	2.6848	1.8849	2.0964	1.6113	1.9307
N_7	0.2344	0.1234	2.3304	2.6840	1.8843	2.0958	1.6112	1.9301
N_8	0.2344	0.1234	2.3307	2.6840	1.8846	2.0958	1.6114	1.9301
N_9	0.4696	0.5284	1.9879	1.9017	1.7243	1.6774	1.2575	1.1750
N_{10}	0.2345	0.1234	2.3307	2.6848	1.8849	2.0964	1.6113	1.9307
N_{15}	0.4675	0.5272	1.9889	1.9006	1.7241	1.6759	1.2592	1.1749
N_{16}	0.2342	0.1228	2.3292	2.6837	1.8832	2.0951	1.6105	1.9303
N_{17}	0.1426	0.1228	2.3292	2.6837	1.8299	2.0951	1.6638	1.9303
N_{20}	0.2355	0.1259	2.3310	2.6846	1.8854	2.0979	1.6110	1.9289
N_{21}	0.2355	0.1259	2.3310	2.6846	1.8854	2.0979	1.6110	1.9289
N_{22}	0.4686	0.5282	1.9868	1.9008	1.7228	1.6766	1.2573	1.1745
N_{27}	0.4698	0.5296	1.9855	1.8983	1.7223	1.6750	1.2559	1.1723
N_{28}	0.2334	0.1224	2.3301	2.6843	1.9421	2.0953	1.6116	1.9310
N_{29}	0.2334	0.1224	2.3301	2.6843	1.9421	2.0953	1.6116	1.9310

expansions are used in the study of electromagnetic fields of charge and current distributions. The efficiency of such a fast method is superior if the system is clustered and has large density fluctuation [79]. So, the lack of experimental demonstration and its importance in theoretical simulations was a motivation for us to investigate dipole moments from a theoretical point of view.

The coefficients of angular coordinates of multipole moment are defined as a sum of following spherical harmonics:

$$f(\theta,\phi)=\sum_{l=0}^{\infty}\sum_{m=-l}^{l}C_l^m Y_l^m(\theta,\phi) \tag{2}$$

So, the electromagnetic potential can be obtained as:

$$\begin{aligned} V&=(r,\theta,\phi)\sum_{i=0}^{\infty}\sum_{m=-l}^{l}C_l^m(r)\,Y_l^m(\theta,\phi)\\ &=\sum_{j=1}^{\infty}\sum_{l=0}^{\infty}\sum_{m=-l}^{l}\frac{D_{l,j}^m}{r^j}\,Y_l^m(\theta,\phi) \end{aligned} \tag{3}$$

The Taylor expansion of $v(r-R)$ around the $r=0$ is,

$$\begin{aligned} V(r-R)&=v(R)-\sum_{\alpha=x,y,z}r_a v_\alpha(R)\\ &\quad+\frac{1}{2}\sum_{\alpha=x,y,z}\sum_{\beta=x,y,z}r_\alpha r_\beta v_{a\beta}(R)-\cdots+\cdots \end{aligned} \tag{4}$$

where,

$$V_\alpha(R)=\left(\frac{\partial v(r-R)}{\partial r_a}\right)\quad\text{and}\ V_{\alpha\beta}(R)=\left(\frac{\partial^2 v(r-R)}{\partial r_\alpha \partial r_\beta}\right)_{r=0} \tag{5}$$

So, the above equation can be considered as the differential of v in terms of r.

Interaction of two non-overlapping parts of BNB and $B_{15}N_{15}$ The total electrostatic interaction energy of the system considered ($U_{B_{15}N_{15}-BNB}$) between the two charge distributions is

$$U_{B_{15}N_{15}-BNB}=\sum_{\mu\in B_{15}N_{15}}\sum_{v\in BNB}\frac{q_\mu q_v}{4\pi\varepsilon_0 r_{\mu v}} \tag{6}$$

As a consequence of the electrostatic $B_{15}N_{15}$–BH_2NBH_2 interaction, the charge distribution of the BNB molecule, inside the $B_{15}N_{15}$ ring polarizes the $B_{15}N_{15}$ charge distribution and induces are electromagnetic fields in the $B_{15}N_{15}$–BH_2NBH_2 system.Considering $r_{XY}=r_Y-r_X$, it can be defined as:

$$R_{B_{15}N_{15}-BNB}+r_{BNB,v}+r_{v\mu}-r_{\mu,B_{15}N_{15}}=0 \tag{7}$$

Since the two distributions do not overlap:

$$\left|R_{B_{15}N_{15}-BNB}\right|\ >\left|r_{BNB,v}-r_{B_{15}N_{15},\mu}\right| \tag{8}$$

The Laplace expansion could be considered as:

$$\begin{aligned} \frac{1}{|r_v-r_\mu|}&=\frac{1}{\left|R_{B_{15}N_{15}-BNB}-(r_{B_{15}N_{15},\mu}-r_{BNB,v})\right|}\\ &=\sum_{L=0}^{\infty}\sum_{M=-L}^{L}(-1)^M I_L^{-M}(R_{B_{15}N_{15}-BNB})R_L^M\\ &\quad\times(r_{B_{15}N_{15},\mu}-r_{BNB,v}) \end{aligned} \tag{9}$$

where, I_L^M and R_L^M are irregular and regular solid harmonics, respectively. The Dipole moment can be measured by a variety of experimental methods or

Table 5 Total atomic charges, spin densities, electric potential, and isotropic fermi coupling constants of cationic and anionic forms of BNB in different loops and bonds of $B_{15}N_{15}$–BH_2NBH_2 system with EPR-II basis set

$B_{15}N_{15}$–BH_2NBH_2	Anion						Cation					
	Total atomic charges	Total atomic spin densities	Electric potential	Isotropic Fermi coupling MHz	Dipole orientation θ φ	$\Delta V = V_2 - V_1$	Total atomic charges	Total atomic spin densities	Electric potential	Isotropic Fermi coupling MHz	Dipole orientation θ φ	$\Delta V = V_2 - V_1$
Loop 1												
B(18)	−0.23225	0.697368	−11.5799	298.0982			0.052309	–	−11.1317	–		
N(20)	−0.12107	0.000253	−18.5969	48.84742			0.066331	–	−18.2060	–		
N(21)	−0.12097	0.000113	−18.5969	48.84896	141.38		0.065908	–	−18.2064	–	51.21	
B(23)	−0.07780	0.135312	−11.5979	82.38171	123.87		0.021456	–	−11.2116	–	67.28	
B(24)	−0.07794	0.135228	−11.5979	82.37310			0.021229	–	−11.2116	–		
N(27)	−0.31230	0.016496	−18.5741	14.35820			−0.03210	–	−18.2137	–		
Bond1												
N(15)	−0.38733	0.553445	−18.6118	−4.54714	109.03	21.28	0.050086	–	−18.1622	–	29.23	−134.60
B(18)	−0.43441	0.579329	−11.6277	148.5433	129.46		0.048930	–	−11.1569	–	82.42	
Loop 2												
B(5)	−0.23638	0.692043	−11.5770	298.5955			0.043491	–	−11.1359	–		
N(7)	−0.11906	0.006735	−18.5924	48.95212			0.076052	–	−18.2071	–		
N(8)	−0.11860	0.006746	−18.5924	48.94548	69.83		0.076240	–	−18.2072	–	120.96	
B(11)	−0.07676	0.132758	−11.5947	82.05908	132.44		0.011610	–	−11.2127	–	64.77	
B(12)	−0.07597	0.132713	−11.5947	82.06147			0.012115	–	−11.2127	–		
N(15)	−0.29341	0.014298	−18.5727	14.00687			−0.03003	–	−18.2125	–		
Bond2												
N(2)	−0.41496	0.431074	−18.6211	−5.60251	36.39	20.46	0.024322	–	−18.1740	–	88.62	−589.53
B(5)	−0.47667	0.574238	−11.6373	137.4786	133.97		0.070712	–	−11.1509	–	61.41	
Loop 3												
B(1)	−0.07714	0.134777	−11.5956	82.94055			0.023138	–	−11.2072	–		
N(2)	−0.30719	0.012734	−18.5726	14.45047			−0.01730	–	−18.1963	–		
N(3)	−0.12272	0.004923	−18.5930	49.12203	4.43		0.066599	–	−18.2015	–	151.48	
B(4)	−0.07744	0.134833	−11.5956	82.93281	40.08		0.022883	–	−11.2072	–	167.72	
B(6)	−0.22623	0.688839	−11.5777	299.4035			0.046411	–	−11.1302	–		
N(10)	−0.22623	0.004961	−18.5930	49.12040			0.066749	–	−18.2014	–		
Bond3												
N(9)	−0.38883	0.525549	−18.6151	−4.93362	39.93	21.75	0.042860	–	−18.1637	–	163.17	−244.11
B(6)	−0.44529	0.591569	−11.6294	147.3592	42.26		0.062077	–	−11.1541	–	112.86	

Table 5 continued

$B_{15}N_{15}$–BH_2NBH_2	Anion						Cation					
	Total atomic charges	Total atomic spin densities	Electric potential	Isotropic Fermi coupling MHz	Dipole orientation θ φ	$\Delta V = V_2 - V_1$	Total atomic charges	Total atomic spin densities	Electric potential	Isotropic Fermi coupling MHz	Dipole orientation θ φ	$\Delta V = V_2 - V_1$
Loop 4												
N(9)	−0.30220	0.012676	−18.5487	14.10025			−0.02309	–	−18.2064	–		
B(13)	−0.08345	0.133245	−11.6158	81.90976			0.008490	–	−11.2104	–		
B(14)	−0.08322	0.133200	−11.6158	81.90746	79.35		0.008576	–	−11.2102	–	75.32	
N(16)	−0.12100	0.004170	−18.5866	48.93729	41.03		0.070577	–	−18.2033	–	152.32	
N(17)	−0.12083	0.004124	−18.5867	48.95524			0.069639	–	−18.2044	–		
B(19)	−0.24254	0.698117	−11.4689	297.1314			0.052149	–	−11.1305	–		
Bond4												
N(22)	−0.39698	0.498184	−18.6148	−5.26185	112.28	20.64	0.047943	–	−18.1640	–	101.14	−205.15
B(19)	−0.44303	0.597204	−11.6289	152.8920	38.24		0.064208	–	−11.1540	–	150.96	
Loop 5												
N(22)	−0.29553	0.013937	−18.5717	14.16785			0.011335	–	−18.1716	–		
B(25)	−0.07267	0.134030	−11.5935	82.55659			0.030322	–	−11.1978	–		
B(26)	−0.07306	0.133954	−11.5935	82.53802	148.31		0.029851	–	−11.1978	–	25.39	
N(28)	−0.11844	0.005227	−18.5905	49.14651	30.01		0.079816	–	−18.1926	–	172.80	
N(29)	−0.11834	0.005217	−18.5905	49.14699			0.079614	–	−18.1928	–		
B(30)	−0.23276	0.690523	−11.5759	300.2759			0.036972	–	−11.1273	–		
Bond5												
N(27)	−0.39628	0.501982	−18.6090	−4.80386	171.93	21.70	0.054897	–	−18.1540	–	38.15	−490.41
B(30)	−0.46062	0.558831	−11.6306	135.3680	44.71		0.069811	–	−11.1502	–	162.20	

$B_{15}N_{15}$–BH_2NBH_2	Radical					
	Total atomic charges	Total atomic spin densities	Electric potential	Isotropic Fermi coupling MHz	Dipole orientation θ φ	$\Delta V = V_2 - V_1$
Loop 1						
B(18)	0.022773	0.007771	−11.2912	1.92951		
N(20)	0.020236	−0.00167	−18.3614	0.06510		
N(21)	0.020184	−0.00168	−18.3614	0.06565	137.70	
B(23)	0.018498	0.001483	−11.3661	0.15582	39.89	
B(24)	0.018329	0.001421	−11.3662	0.16040		
N(27)	−0.10748	−0.00148	−18.3720	−0.17787		

Table 5 continued

$B_{15}N_{15}$–BH_2NBH_2	Radical					
	Total atomic charges	Total atomic spin densities	Electric potential	Isotropic Fermi coupling MHz	Dipole orientation θ φ	$\Delta V = V_2 - V_1$
Bond1						
N(15)	−0.02491	0.983539	−18.3265	79.89108	35.40	1386.85
B(18)	0.017355	−0.96774	−11.3047	−1113.72	141.43	
Loop 2						
B(5)	0.016290	0.000699	−11.2889	1.60375		
N(7)	0.022423	−0.00091	−18.3583	0.16205		
N(8)	0.022759	−0.00091	−18.3583	0.16167	149.93	
B(11)	0.014967	0.001946	−11.3646	0.53875	128.37	
B(12)	0.015577	0.001938	−11.3646	0.53804		
N(15)	−0.09393	−0.00002	−18.3717	0.23242		
Bond2						
N(2)	−0.02087	0.985227	−18.3210	81.12607	43.12	1417.07
B(5)	0.020945	−0.97843	−11.2990	−1130.26	48.83	
Loop 3						
B(1)	0.017866	0.000604	−11.3646	0.24929		
N(2)	−0.10561	−0.00095	−18.3705	−0.15070		
N(3)	0.019620	−0.00070	−18.3582	−0.32147	82.08	
B(4)	0.017653	0.000607	−11.3646	0.24837	136.09	
B(6)	0.026818	0.002521	−11.2886	1.36305		
N(10)	0.019679	−0.00072	−18.3582	−0.32250		
Bond3						
N(9)	−0.01838	1.000211	−18.3245	82.35464	113.41	1542.24
B(6)	0.020712	−0.99371	−11.3024	−1132.75	42.63	
Loop 4						
N(9)	−0.10107	−0.00026	−18.3738	0.19133		
B(13)	0.009870	0.002286	−11.3672	0.16583		
B(14)	0.010114	0.002313	−11.3672	0.16500	4.13	
N(16)	0.021679	−0.00067	−18.3620	0.75611	126.18	
N(17)	0.021875	−0.00068	−18.3620	0.75536		
B(19)	0.013141	0.004387	−11.2921	1.95322		
Bond4						
N(22)	−0.03999	−0.95948	−18.3303	−78.1267	171.76	1919.96
B(19)	0.007737	0.989324	−11.3087	1110.837	14.83	

Table 5 continued

$B_{15}N_{15}$–BH_2NBH_2	Radical						
	Total atomic charges	Total atomic spin densities	Electric potential	Isotropic Fermi coupling	Dipole orientation		$\Delta V = V_2 - V_1$
				MHz	θ	φ	
Loop 5							
N(22)	−0.09476	−0.00025	−18.3698	−0.08428			
B(25)	0.022091	0.000466	−11.3631	0.28156			
B(26)	0.021675	0.000468	−11.3631	0.28165	59.84		
N(28)	0.020930	−0.00084	−18.3561	−0.32515	46.85		
N(29)	0.020985	−0.00083	−18.3561	−0.32561			
B(30)	0.020570	0.000659	−11.2867	1.13316			
Bond5							
N(27)	−0.03201	−0.96068	−18.3321	−78.7892	115.40		−3659.90
B(30)	−0.00267	0.986277	−11.3092	1106.590	132.85		

computed with atomic charge distribution directly derived from molecular orbital calculations. So, the interaction energy of $B_{15}N_{15}$ and BNB charge distribution, with a distance $R_{B_{15}N_{15}-BNB}$ apart. Since,

$$I_{l_{B_{15}N_{15}}+l_{BNB}}^{-(m_{B_{15}N_{15}}+m_{BNB})}(R_{B_{15}N_{15}-BNB}) = \left[\frac{4\pi}{2l_{B_{15}N_{15}}+2l_{BNB}+1}\right]^{1/2} \frac{Y_{l_{B_{15}N_{15}}+l_{BNB}}^{-(m_{B_{15}N_{15}}+m_{BNB})}(\hat{R}_{B_{15}N_{15}-BNB})}{l_{B_{15}N_{15}}+l_{BNB}+1} \quad (10)$$

A dipole moment which appear, because of an electric charge distribution usually involves powers (or inverse powers) of the distance to the origin (r) as well as some angular dependence (Θ and Φ), where Θ is the angle with the x and y axes and Φ is the angle with the vertical axis inside the ring [79, 80]. Dipole moment converges under two conditions: (1) if the charges are localized close to the origin and the point at which the potential is observed is far from the origin where the coefficients of the series expansion are called exterior dipole moments or simply dipole moments (2) if the charges are located far from the origin and the potential is observed close to the origin, namely interior dipole moments. The importance of this quantity is embedded in this fact that the potential at a position within a charge distribution can often be computed by combining interior and exterior dipoles [78–80]. When a single BNB molecule is just considered $\Theta = \Phi = 0$, i.e., the dipole vector to be coincident with the BNB axis. According to the dipole moments obtained, it can be distinguished that the r component of the dipole moment vector of each radical cationic and anionic forms of BNB involved in the ring had the tendency to rotate in three different conical surfaces. So, it could be realized that our observed dipole moment has been directed linearly and this observation supported the intrinsic linear form of BNB molecule.

In this regard, it seems that if a biomolecule is set in the BNB–$B_{15}N_{15}$ system because of generation of radical, anion, and cation forms of BNB the electrical current will cross along the ring that changes all calculated atomic physico-chemical properties. Here, it is notable that the three emerged radical, cationic, and anionic forms of BNB generate frequently to each other and if these three species are imagined in the three quantized cone surfaces it can be deduced that the variation of the radial vector of dipole moment (r) of the system would be quantized when crossing these three cone levels.

An induced dipole of any polarizable charge distribution ρ of the BNB molecule is caused by an electric field external to ρ that originates from an ion or polar molecule in the vicinity of ρ. The strength of the induced dipole is equal to the product of the strength of the external field and

Table 6 Total atomic charges, spin densities, electric potential, and isotropic fermi coupling constants of cationic and anionic forms of BNB in different loops and bonds of $B_{15}N_{15}$–BH_2NBH_2 system with EPR-III basis set

$B_{15}N_{15}$–BH_2NBH_2	Anion						Cation					
	Total atomic charges	Total atomic spin densities	Electric potential	Isotropic Fermi coupling MHz	Dipole orientation θ φ	$\Delta V = V_2 - V_1$	Total atomic charges	Total atomic spin densities	Electric potential	Isotropic Fermi coupling MHz	Dipole orientation θ φ	$\Delta V = V_2 - V_1$
Loop 1												
B(18)	0.723446	0.557050	−11.5929	285.2066			0.052309	–	−11.1317	–		
N(20)	−1.04645	0.127501	−18.6171	47.32402			0.066331	–	−18.2257	–		
N(21)	−1.04630	0.127283	−18.6171	47.32702	141.11		0.065908	–	−18.2257	–	48.40	
B(23)	0.658351	0.091422	−11.6130	78.13023	123.92		0.021456	–	−11.2267	–	65.92	
B(24)	0.659038	0.091120	−11.6130	78.13017			0.021229	–	−11.2267	–		
N(27)	−0.89674	−0.00799	−18.5952	13.73495			−0.03210	–	−18.2172	–		
Bond1												
N(15)	−0.91804	0.446011	−18.6174	−6.11242	106.84	174.32	−0.42141	–	−18.2266	–	19.91	67.74
B(18)	0.075528	0.689647	−11.6348	168.5806	129.74		0.456754	–	−11.1866	–	121.24	
Loop 2												
B(5)	0.707844	0.554825	−11.5870	285.9986			0.856901	–	−11.1511	–		
N(7)	−1.04769	0.159145	−18.6137	47.26548			−0.74287	–	−18.2318	–		
N(8)	−1.04774	0.158951	−18.6137	47.26345	69.35		−0.74280	–	−18.2318	–	119.70	
B(11)	0.667634	0.087766	−11.6105	77.59551	132.47		0.732637	–	−11.2329	–	64.69	
B(12)	0.668028	0.087585	−11.6105	77.59156			0.733063	–	−11.2329	–		
N(15)	−0.87479	−0.05605	−18.5932	13.27511			−0.66802	–	−18.2285	–		
Bond2												
N(2)	−0.97573	0.243458	−18.6352	−9.14543	33.63	396.03	−0.43149	–	−18.2312	–	67.782	66.50
B(5)	0.030889	0.756168	−11.6432	164.3592	134.13		0.461293	–	−11.1889	–	66.08	
Loop 3												
B(1)	0.652759	0.092279	−11.6147	79.31055			0.747930	–	−11.2305	–		
N(2)	−0.90636	0.010730	−18.5951	14.07795			−0.65860	–	−18.2237	–		
N(3)	−1.00736	0.110192	−18.6192	47.78814	4.59		−0.75813	–	−18.2300	–	149.29	
B(4)	0.653216	0.092246	−11.6147	79.31412	40.51		0.748395	–	−11.2305	–	167.61	
B(6)	0.686389	0.573273	−11.5915	286.9685			0.859040	–	−11.1490	–		
N(10)	−1.00754	0.110135	−18.6192	47.78510			0.758352	–	−18.2300	–		
Bond3												
N(9)	−0.95010	0.335497	−18.6426	−8.15431	42.13	215.04	−0.34874	–	−18.1709	–	164.69	76.02
B(6)	0.059573	0.757939	−11.6420	173.3122	42.48		0.466683	–	−11.1622	–	113.80	

Table 6 continued

$B_{15}N_{15}$–BH_2NBH_2	Anion						Cation					
	Total atomic charges	Total atomic spin densities	Electric potential	Isotropic Fermi coupling MHz	Dipole orientation θ φ	$\Delta V = V_2 - V_1$	Total atomic charges	Total atomic spin densities	Electric potential	Isotropic Fermi coupling MHz	Dipole orientation θ φ	$\Delta V = V_2 - V_1$
Loop 4												
N(9)	−0.89976	−0.03201	−18.5949	13.46105			−0.72475	–	−18.2849	–		
B(13)	0.655792	0.093646	−11.6140	77.58026			0.724112	–	−11.2535	–		
B(14)	0.656175	0.093644	−11.6140	77.57693	79.79		0.724369	–	−11.2535	–	52.79	
N(16)	−1.03030	0.132756	−18.6183	47.24194	40.98		−0.75698	–	−18.2497	–	164.38	
N(17)	−1.03001	0.132809	−18.6183	47.24418			−0.75693	–	−18.2497	–		
B(19)	0.703725	0.563859	−11.5887	284.2143			0.851557	–	−11.1627	–		
Bond4												
N(22)	−0.94901	0.401890	−18.6265	−6.95118	114.44	181.87	−0.41477	–	−18.2231	–	118.31	68.25
B(19)	0.071715	0.688137	−11.6354	161.5190	38.07		0.459920	–	−11.1835	–	156.61	
Loop 5												
N(22)	−0.90606	−0.00674	−18.5949	14.39690			−0.70852	–	−18.2612	–		
B(25)	0.669324	0.083931	−11.6073	80.05284			0.733930	–	−11.2454	–		
B(26)	0.669205	0.083858	−11.6073	80.05472	148.93		0.733833	–	−11.2454	–	21.01	
N(28)	−1.02687	0.141226	−18.6155	47.9875	29.80		−0.74768	–	−18.2408	–	147.14	
N(29)	−1.02676	0.140716	−18.6155	47.98313			−0.74803	–	−18.2408	–		
B(30)	0.685854	0.557498	−11.5944	284.5967			0.846259	–	−11.1613	–		
Bond5												
N(27)	−0.94531	0.384946	−18.6288	−6.99011	171.58	246.39	−0.43117	–	−18.2239	–	55.35	65.93
B(30)	0.051337	0.678690	−11.6377	150.3695	62.20		0.472409	–	−11.1835	–	157.90	

$B_{15}N_{15}$–BH_2NBH_2	Radical					
	Total atomic charges	Total atomic spin densities	Electric potential	Isotropic Fermi coupling (MHz)	Dipole orientation θ φ	$\Delta V = V_2 - V_1$
Loop 1						
B(18)	0.859072	0.008909	−11.3127	1.76961		
N(20)	−0.81373	−0.00538	−18.4034	0.07942		
N(21)	−0.81375	−0.00554	−18.4034	0.07983	139.86	
B(23)	0.742745	0.003245	−11.3851	0.15457	39.59	
B(24)	0.743210	0.003073	−11.3851	0.15717		
N(27)	−0.72884	−0.00152	−18.3838	−0.15413		

Table 6 continued

$B_{15}N_{15}$–BH_2NBH_2	Radical					
	Total atomic charges	Total atomic spin densities	Electric potential	Isotropic Fermi coupling (MHz)	Dipole orientation θ φ	$\Delta V = V_2 - V_1$
Bond1						
N(15)	−0.49429	1.066779	−18.3522	83.67598	34.02	60.50
B(18)	0.484096	−1.05395	−11.3160	−1119.45	141.63	
Loop 2						
B(5)	0.838326	−0.00084	−11.3091	1.64850		
N(7)	−0.79366	0.001324	−18.4009	0.12326		
N(8)	−0.79366	0.001321	−18.4010	0.12342	144.95	
B(11)	0.745692	0.001695	−11.3836	0.48866	129.66	
B(12)	0.746107	0.001694	−11.3836	0.48855		
N(15)	−0.74304	−0.00257	−18.3843	0.22443		
Bond2						
N(2)	−0.50527	1.059581	−18.3535	80.68608	42.08	58.67
B(5)	0.505402	−1.05513	−11.2960	−1102.27	49.02	
Loop 3						
B(1)	0.740392	0.000633	−11.3832	0.26682		
N(2)	−0.72818	0.003057	−18.3826	−0.12225		
N(3)	−0.79776	−0.00312	−18.4004	−0.27290	79.11	
B(4)	0.740801	0.000647	−11.3832	0.26672	136.32	
B(6)	0.847089	0.003463	−11.3098	1.51394		
N(10)	−0.79793	−0.00315	−18.4004	−0.27266		
Bond3						
N(9)	−0.48919	1.078818	−18.3454	84.52569	113.16	60.77
B(6)	0.485820	−1.07303	−11.3064	−1103.69	42.71	
Loop 4						
N(9)	−0.74696	−0.00069	−18.3861	0.19411		
B(13)	0.743004	0.001907	−11.3861	0.17405		
B(14)	0.743235	0.001932	−11.3861	0.17324	5.46	
N(16)	−0.79354	−0.00137	−18.4043	0.68093	92.98	
N(17)	−0.79343	−0.00140	−18.4043	0.68078		
B(19)	0.832737	0.004731	−11.3131	2.06939		
Bond4						
N(22)	−0.47539	−1.05259	−18.3324	−82.9883	175.50	62.59
B(19)	0.470757	1.052052	−11.3123	1089.713	69.69	

Table 6 continued

$B_{15}N_{15}$–BH_2NBH_2	Radical					
	Total atomic charges	Total atomic spin densities	Electric potential	Isotropic Fermi coupling (MHz)	Dipole orientation θ φ	$\Delta V = V_2 - V_1$
Loop 5						
N(22)	−0.73655	0.000199	−18.3827	−0.05100		
B(25)	0.737488	−0.00040	−11.3818	0.32111		
B(26)	0.737300	−0.00042	−11.3818	0.32136	64.58	
N(28)	−0.79081	0.001063	−18.3985	−0.21220	46.42	
N(29)	−0.79124	0.001052	−18.3985	−0.21211		
B(30)	0.850145	0.000416	−11.3071	1.31074		
Bond5						
N(27)	−0.46431	−1.06964	−18.3264	−86.6213	101.79	64.11
B(30)	0.459043	1.066792	−11.3119	1083.921	134.67	

the dipole polarizibility of ρ. So, along with the variation of the radial component, (r) the two other remaining components of the dipole moment, namely, Θ and Φ will be changed and causes the quantized rotation of BNB molecule. Due to the electrical charge of BNB and its induced electrostatic interaction the ring will be affected and the rotation of $B_{15}N_{15}$ ring is also expected to be quantized.On the other hand, for a dipole moment (m) the energy of the dipole interaction (U) is defined as [78–80]:

$$U = -m \cdot B \tag{11}$$

The BNB radical had the highest dipole moment at −15.0° (5.0998 Debye) and at −135.0°, while at −135.0° the lowest dipole moment was evident. The dipole moment variation at different rotational angles showed that from −135.0 to −30° the increasing trend of dipole moment was evident and the maximum point was at −30° and dramatically decreased and then increase of dipole moment value has been observed from −30° up to +30°.

The average value of the radical component of the dipole moment vector (r) for anion, cation, and radical forms of BNB have been obtained as 14.79, 4.10, and 1.94 Debye, respectively. Along with the high values of Θ, Φ the r of dipole moment holds a Gaussian distribution, this fact can be observed in the plotted Gaussian graphs of dipole moment (r) versus Θ and Φ angles (Fig. 2). Here, it is interesting that for each radical, cation, and anion of BNB three individual expectation values of $\langle \Delta E \rangle$, $\langle \Delta V \rangle$, and $\langle \Delta r \rangle$ have been obtained and as a whole it seems that the r component of dipole moment of the system, voltage differences, and relative energies quantized and the system undergoes quantization through rotation.

Electromagnetic hyperfine parameters

DFT methods (particularly B3LYP) with EPR-II and EPR-III basis sets seemed evidence for their suitable theoretical model for the computation of hyperfine coupling constants. Total atomic charges, spin densities, electric potential, and isotropic Fermi coupling constants of cationic and anionic forms of BNB in different loops and bonds of the $B_{15}N_{15}$–BNB system with EPR-III and EPR-III basis sets have been reported listed in Tables 5 and 6. Also, the relative energies (ΔE), radial coordinate of dipole moment (r) as well as the voltage differences (ΔV) and rotation of the BH_2NBH_2–$B_{15}N_{15}$ system with $\langle \Delta r_{r-c} \rangle = 1.831645107$ Debye, $\langle \Delta r_{r-a} \rangle = 12.51807427$ Debye, $\langle \Delta r_{a-c} \rangle = 10.686429163$ Debye, $\langle \Delta E_{a-c} \rangle = 0.4775024$ Hartree $\langle \Delta E_{a-r} \rangle = 0.115731$ Hartree, $\langle \Delta E_{c-r} \rangle = 0.3617714$ Hartree and adenine–BNB–thymine with $\langle \Delta E_{r-c} \rangle = 0.083$ Hartree, $\langle \Delta E_{r-a} \rangle = 0.079441$ Hartree and $\langle \Delta E_{a-c} \rangle = 0.003559$ Hartree have been reported in Table 7.

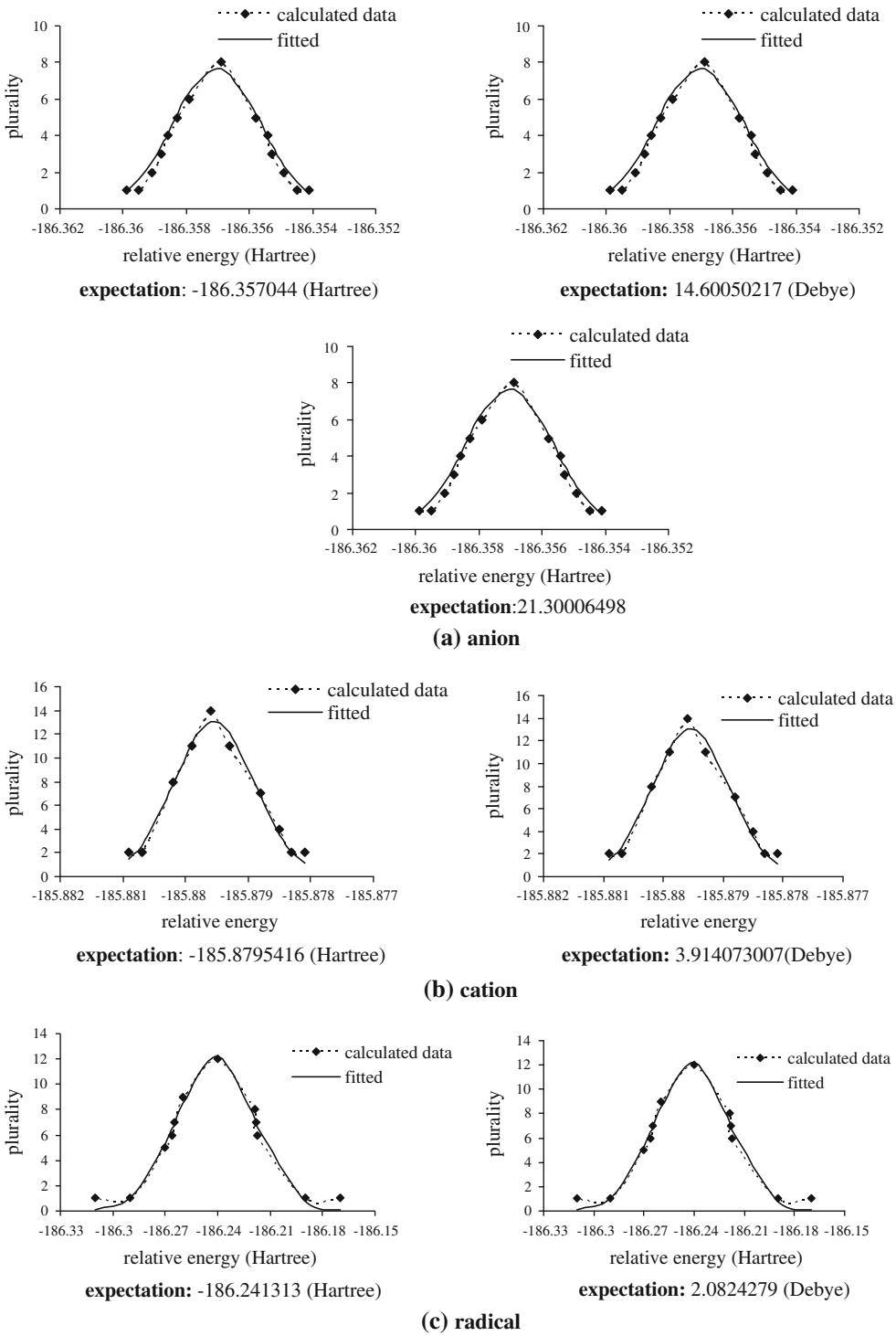

Fig. 2 The gaussian distributions and expectation values of quantized radical coordinate of dipole moment, voltage differences (a.u.) and relative energies of $B_{15}N_{15}$–BH_2NBH_2 systems at the level of B3LYP/EPR-II of theory

The voltage (ΔV) variations between two atoms involved in each bond of $B_{15}N_{15}$ gave useful structural information. In the case of the BNB anion, these values were close to each other. The reason is that because of induction the high structural stability of the BH_2NBH_2 anion to the $B_{15}N_{15}$ ring the electron density of each of the five rings in $B_{15}N_{15}$ has been distributed in a homogenous way and yielded the voltage differences close together.

All the voltage differences (ΔV) of five different bonds of the BNB anion with both EPR-II and EPR-III basis sets were close together and varied in a range of 20.64 and 21.75 a.u. to 174.32 up to 396.03 a.u., respectively. In spite

Table 7 The part of data including relative energies (ΔE), radial coordinate of dipole moment (r) as well as the voltage differences (ΔV) and rotation of BH_2NBH_2–$B_{15}N_{15}$ system with $\langle \Delta r_{r-c} \rangle = 1.831645107$ Debye, $\langle \Delta r_{r-a} \rangle = 12.51807427$ Debye, $\langle \Delta r_{a-c} \rangle = 10.686429163$ Debye, $\langle \Delta E_{a-c} \rangle = 0.4775024$ Hartree $\langle \Delta E_{a-r} \rangle = 0.115731$ Hartree, $\langle \Delta E_{c-r} \rangle = 0.3617714$ Hartree and adenine–BNB–thymine with $\langle \Delta E_{r-c} \rangle = 0.083$ Hartree, $\langle \Delta E_{r-a} \rangle = 0.079441$ Hartree and $\langle \Delta E_{a-c} \rangle = 0.003559$ Hartree

$B_{15}N_{15}$–BH_2–NBH_2	0.0, 0.0, 0.0			0.0, 0.0, 10.0		
	r	$\Delta E_{relative} = E - E_0$ (kcal/mol)	ΔV	r	$\Delta E_{relative} = E - E_0$ (kcal/mol)	ΔV
Anion						
2,5-BNB	14.7644	−2.15	20.46032433	15.9178	−2.19	20.71523624
6,9-BNB	13.6579	0 ($E_0 = -116938.33$)	21.75803896	14.1925	−0.35	22.6200658
15,18-BNB	14.2597	−0.19	21.2846597	14.8319	0 ($E_0 = -116938.29$)	21.04515849
19,22-BNB	14.8677	−1.67	20.64255344	13.4322	−1.32	20.89816549
27,30-BNB	15.6927	−1.54	21.7048069	14.7847	−1.90	21.3463658
Cation						
2,5-BNB	3.7492	−0.64	589.5300526	4.8547	−0.90	163.1095659
6,9-BNB	3.2387	−0.51	244.1107249	4.5002	−0.78	129.3827659
15,18-BNB	4.5531	0 ($E_0 = -116639.10$)	134.6038303	4.1595	0 ($E_0 = -116638.94$)	76.54435468
19,22-BNB	3.9439	−0.63	205.1512785	3.4191	−0.41	84.51828241
27,30-BNB	4.9229	−1.09	170.9726777	3.095	−1.11	1304.528298
Radical						
2,5-BNB	2.2096	−0.86	1417.0732	1.8857	−30.06	691.2087828
6,9-BNB	2.1917	0 ($E_0 = -116852.05$)	1542.246048	1.8597	−28.64	690.5230005
15,18-BNB	2.2292	−0.36	1386.859094	2.2229	0 ($E_0 = -116852.27$)	1405.371096
19,22-BNB	2.3567	−1.06	1919.968463	2.0393	−26.54	569.6730288
27,30-BNB	2.3421	−0.65	−3659.902709	1.8441	−29.74	871.294362
$B_{15}N_{15}$–BH_2–NBH_2	0.0, 0.0, 30.0			0.0, 0.0, 50.0		
	r	$\Delta E_{relative} = E - E_0$ (kcal/mol)	ΔV	r	$\Delta E_{relative} = E - E_0$ (kcal/mol)	ΔV
Anion						
2,5-BNB	15.1797	−1.95	20.88297616	14.8938	−1.20	20.88871963
6,9-BNB	14.3994	−1.36	21.76042379	14.8251	−1.95	21.56229155
15,18-BNB	14.8295	0 ($E_0 = -116938.24$)	21.76669527	15.2197	−0.71	21.6677078
19,22-BNB	13.284	−0.47	21.12789772	13.2976	0 ($E_0 = -116938.22$)	21.2050066
27,30-BNB	15.0909	−2.24	21.2692432	14.747	−2.20	21.5915547
Cation						
2,5-BNB	4.8947	−0.61	140.6631536	4.959	−0.02	41.55647803
6,9-BNB	4.3384	−0.98	267.6288192	4.2686	−0.76	280.3315245

Table 7 continued

$B_{15}N_{15}$–BH_2–NBH_2	0.0, 0.0, 30.0			0.0, 0.0, 50.0		
	r	$\Delta E_{relative} = E - E_0$ (kcal/mol)	ΔV	r	$\Delta E_{relative} = E - E_0$ (kcal/mol)	ΔV
15,18-BNB	3.9786	−0.34	209.6999384	4.5348	−0.70	109.6994096
19,22-BNB	3.2571	0 ($E_0 = -116639.04$)	158.460722	3.4207	0 ($E_0 = -116639.13$)	185.0014562
27,30-BNB	2.3445	−0.40	727.1080127	3.3544	−0.64	37.2229976
Radical						
2,5-BNB	0.4431	0 ($E_0 = -116790.56$)	1132.472196	1.8938	−30.24	654.6874955
6,9-BNB	1.832	−91.20	822.6973169	1.8393	−30.16	867.9263503
15,18-BNB	2.2237	−61.74	1337.729871	2.3704	0 ($E_0 = -116639.13$)	1305.613775
19,22-BNB	2.2325	−61.94	1341.695835	1.8749	−29.30	655.7681642
27,30-BNB	2.2059	−62.32	1537.97237	1.8876	−30.54	687.758719

$B_{15}N_{15}$–BH_2–NBH_2	0.0, 0.0, 70.0			0.0, 0.0, 80.0		
	r	$\Delta E_{relative} = E - E_0$ (kcal/mol)	ΔV	r	ΔE	ΔV
Anion						
2,5-BNB	14.8127	−0.20	21.17170219	14.6757	0 ($E_0 = -116938.10$)	22.77265027
6,9-BNB	15.1978	−2.10	20.53714588	15.0961	−2.42	20.26891353
15,18-BNB	15.517	−1.45	21.39751028	15.6829	−2.06	21.17336468
19,22-BNB	13.3412	0 ($E_0 = -116938.34$)	21.73188441	13.5959	−0.75	20.93999193
27,30-BNB	14.1704	−1.78	20.9271384	14.0317	−1.69	20.9223387
Cation						
2,5-BNB	4.6471	0 ($E_0 = -116639.05$)	169.7753053	4.6651	0 ($E_0 = -116938.04$)	107.587404
6,9-BNB	4.6943	−0.45	184.9872411	4.227	−0.74	252.5279696
15,18-BNB	4.2126	−0.94	373.8859058	4.4664	−0.76	133.8028107
19,22-BNB	3.3545	−0.42	208.2188936	3.4027	−0.67	150.2979356
27,30-BNB	3.1589	−0.65	219.0748971	3.513	−0.27	61.6957402
Radical						
2,5-BNB	1.855	−28.57	682.6710955	2.2283	0 ($E_0 = -116852.22$)	1382.467941
6,9-BNB	2.2053	−0.22	1426.417133	2.2514	−0.85	1271.552389
15,18-BNB	2.3605	0 ($E_0 = -116852.64$)	−1319.57734	1.8369	−29.58	841.5485097
19,22-BNB	1.8592	−28.91	748.2625334	1.8519	−29.34	784.6104379
27,30-BNB	1.8911	−29.64	651.522473	2.2232	−0.61	1153.38002

Table 7 continued

$B_{15}N_{15}$–BH_2–NBH_2	0.0, 0.0, 100.0			0.0, 0.0, 120.0		
	r	ΔE	ΔV	r	ΔE	ΔV
Anion						
2,5-BNB	14.844	0 ($E_0 = -116938.20$)	21.7185532	15.2452	−0.65	21.34933812
6,9-BNB	14.2714	−1.98	20.92690523	13.9859	−1.20	20.875789
15,18-BNB	16.0364	−2.21	21.00412536	15.7689	−2.20	21.22102908
19,22-BNB	13.9105	−1.27	21.75886242	14.2300	−1.90	21.40632195
27,30-BNB	13.9218	−0.65	20.6949306	13.9004	0 ($E_0 = -116938.27$)	21.0987403
Cation						
2,5-BNB	4.898	−0.32	121.1624472	5.0473	−0.74	81.6428792
6,9-BNB	4.2981	−0.65	225.1644614	4.5264	−0.05	37.00481049
15,18-BNB	3.2199	−0.33	837.6064657	4.0462	−0.88	272.2238578
19,22-BNB	3.5329	−0.93	164.757683	3.4077	−0.89	171.4841157
27,30-BNB	3.1799	0 ($E_0 = -116639.04$)	79.51516239	4.1436	0 ($E_0 = -116639.09$)	151.3743912
Radical						
2,5-BNB	1.8415	−288.50	750.8598409	1.8506	−28.25	699.5660606
6,9-BNB	2.3581	−260.54	1479.0878	2.2251	−0.16	1176.821483
15,18-BNB	1.8741	−289.56	793.5420423	1.8849	−29.74	690.6190481
19,22-BNB	17.8652	0 ($E_0 = -116592.60$)	−68.88810583	2.2133	0 ($E_0 = -116852.62$)	1982.734438
27,30-BNB	2.4928	−259.61	887.058866	1.8794	−28.65	670.548603
$B_{15}N_{15}$–BH_2–NBH_2	0.0, 0.0, 140.0			0.0, 0.0, 160.0		
	r	ΔE	ΔV	r	ΔE	ΔV
Anion						
2,5-BNB	15.5314	−1.4	21.40871657	15.8874	−2.21	20.85056244
6,9-BNB	13.9070	−0.28	20.90979922	13.9078	0 ($E_0 = -116938.05$)	21.11771247
15,18-BNB	15.1228	−1.83	20.88366855	14.8768	−1.25	20.97912455
19,22-BNB	14.4024	−2.01	22.15802737	14.2194	−2.33	20.51458781
27,30-BNB	13.9186	0 ($E_0 = -116938.33$)	21.8549812	14.3687	−1.05	21.342321
Cation						
2,5-BNB	5.036	−0.88	142.2312198	4.6421	−0.77	281.9326428
6,9-BNB	4.2957	0 ($E_0 = -116639.11$)	172.6622718	4.3196	−0.18	214.6453227
15,18-BNB	4.1066	−0.59	226.0772618	4.4443	0 ($E_0 = -116639.11$)	48.17624555
19,22-BNB	2.9687	−0.51	247.8705152	3.3449	−0.67	183.4943225
27,30-BNB	3.4375	−0.43	131.927256	3.5383	−0.66	80.12520977

Table 7 continued

$B_{15}N_{15}$–BH_2–NBH_2	0.0, 0.0, 140.0			0.0, 0.0, 160.0		
	r	ΔE	ΔV	r	ΔE	ΔV
Radical						
2,5-BNB	2.1681	0 ($E_0 = -116852.37$)	1872.57265	2.1959	−0.81	1753.814514
6,9-BNB	1.8831	−29.35	700.1523844	1.8821	−29.38	668.2052501
15,18-BNB	1.8889	−29.93	644.3979797	2.235	−0.94	1214.141799
19,22-BNB	1.8708	−29.84	778.5549349	1.9333	−30.49	587.9741464
27,30-BNB	1.8735	−29.03	706.02263	2.3876	0 ($E_0 = -116851.79$)	1477.15994

	Expectation values		
Anion	$\langle r \rangle = 14.60050217$ (Debye)	$\langle E \rangle = -186.357044$ (Hartree)	$\langle V \rangle = 21.30006498$ (a.u.)
Cation	$\langle r \rangle = 3.914073007$ (Debye)	$\langle E \rangle = -185.8795416$ (Hartree)	
Radical	$\langle r \rangle = 2.0824279$ (Debye)	$\langle \mathrm{E} \rangle = -186.241313$ (Hartree)	

$B_{15}N_{15}$–A–BNB–T	Anion			Cation			Radical		
	r	ΔE	ΔV	r	ΔE	ΔV	r	ΔE	ΔV
2,5-A–BNB–T	14.1363	−1106.749613	32.87940598	20.3745	−1106.3830501	744.876442	15.1582	−1106.6921017	−1189.821498
6,9-A–BNB–T	14.1259	−1106.759704	30.73110087	20.7348	−1106.3869194	−4837.350231	14.8793	−1106.6867881	235.934259
15,18-A–BNB–T	13.1638	−1106.78462	31.97708898	19.5124	−1106.3812639	7566.22623	9.1569	−1106.6539139	−367.6868112
19,22-A–BNB–T	1.6871	−1106.7631563	−75.1917668	18.8879	−1106.3942203	−6817.238387	13.3051	−1106.680072	−3574.055444
27,30-A–BNB–T	7.6835	−1106.7759362	15.12004243	18.5529	−1106.3815378	−142.9915417	14.1905	−1106.6804865	−2090.705381
1,2,3,4,6,10-A–BNB–T	15.0938	−1266.1729359	–	19.3854	−1265.8525377	–	16.0051	−1266.1096218	–
5,7,8,11,12,15-A–BNB–T	22.8012	−1266.1793463	–	18.2938	−1265.8598774	–	14.5887	−1266.1177917	–
9,13,14,16,17,19-A–BNB–T	6.4011	−1266.0498516	–	14.1555	−1265.7427315	–	11.6559	−1265.978766	–
18,20,21,23,24,27-A–BNB–T	14.3638	−1266.1725841	–	18.9363	−1265.8478929	–	14.8208	−1266.107705	–
22,25,26,28,29,30-A–BNB–T	7.4840	−1266.1188578	–	18.8367	−1265.8020106	–	10.9272	−1266.0609021	–

of these close anionic ΔV values, for BNB cation and radical the range of ΔV variations with the EPR-II basis set are more considerable, i.e., for BNB cation and radical the ΔV values were −589.53 up to −134.60 a.u. and −3659.90 up to 1919.96 a.u., respectively. However, with the EPR-III basis set the corresponding values of the BNB cation and radical were in a specific range of 65.93 and 76.02 a.u. and 58.67 up to 64.11 a.u., respectively. Hence, closeness of ΔV values of BNB anion with both EPR-II and EPR-III basis sets may refer to the higher structural stability of BNB anion inside the B15N15 ring which supports the higher HOMO–LUMO band gap value for BNB anion (26.9 a.u.).

For the BNB radical, all ΔV values were positive except for bond 5 of BNB radical that yielded a high negative value ($\Delta V = -3659.90$ a.u.). In the case of ΔV values with the EPR-III basis the most positive ΔV (64.11 a.u.) was also related to this bond 5.

Moreover, for further investigation of the extent of ΔV variation, the average values of ΔV of each form as the expectation values $\langle \Delta E \rangle$, $\langle \Delta V \rangle$, and $\langle \Delta r \rangle$ have been evaluated. According to the plotted graphs (see Fig. 2; Table 7), the ΔV data were obeyed a Gaussian distribution and the comparison of the sharpness of these Gaussian curves exhibited the extent of ΔV variation. In the case of the BNB anion the average ΔV values with both EPR-II basis sets were 21.17 a.u. The expectation value of $\langle \Delta E \rangle$, $\langle \Delta V \rangle$, and $\langle \Delta r \rangle$ coordinate for the anion case were −186.357044 Hartree, 21.30006498 a.u., and 14.60050217 Debye, respectively. However, the corresponding average values of ΔV of BNB cation and radical with EPR-II basis set were −332.761 a.u., and 1774.478 a.u. and with EPR-III basis sets for cation and radical these average values were 68.892 and 48.812 a.u., respectively. The expectation values of $\langle r \rangle$ coordinates for the cation were −185.8795416 Hartree and 3.9017 Debye. Also, the expectation value of $\langle \Delta E \rangle$ and $\langle r \rangle$ coordinates for BNB radical were −186.241313 Hartree and 2.0824 279 Debye, respectively. From the basis set effect on these values the following points can be seen: first, the average value of ΔV especially for the BNB anion showed a considerable increase from 21.17 up to 242.73 a.u. Also, the similar trend occurs for the BNB cation, i.e., the average ΔV increases from −332.76 up to 68.89 a.u. Conversely, the decrease of this average ΔV value has been observed from 1774.47 to 48.81 a.u. Therefore, the fluctuations of ΔV values especially in BNB cation were considerable and deviated from the supposed sharp Gaussian distribution. Hence, as it was expected the Gaussian curve of BNB anion was sharper than the corresponding values of the cationic and radical forms.

It is interesting that the corresponding isotropic Fermi contact coupling of the anionic form the EPR-II basis set also changed between −5.60251 up to 300.2759 MHz and with EPR-III basis set varied from −9.14543 up to 286.9685 MHz which its variation's range corresponded to L-bond that is why the bond voltage (ΔV) remained constant and have not exhibited significant fluctuation.

The calculation of the IFC in the cationic state was impossible and in this case no data were available to analysis. The reason for the high positive values obtained for isotropic Fermi coupling for B atoms in comparison with N atoms in the system considered is that the region of our system containing nitrogen atoms was thicker than the B atoms. Hence, the charge transfer tended to orient along with the direction of rotation of the BNB molecule. The important point is that around each loop an electromagnetic field has been intensified along with bonds and caused the loop's rotation from the direction of N atom to the B atom.

All the bonding IFC values of B atoms the derived by the EPR-II basis set were positive. Although this fact was not true for the EPR-III basis set and for radical case the similar trends have been obtained as:

For EPR-II basis set:

$$\mathrm{IFC_{bond4}} > \mathrm{IFC_{bond5}} > \mathrm{IFC_{bond3}} > \mathrm{IFC_{bond2}} > \mathrm{IFC_{bond1}}$$

For EPR-III basis set:

$$\mathrm{IFC_{bond4}} > \mathrm{IFC_{bond5}} > \mathrm{IFC_{bond3}} > \mathrm{IFC_{bond1}} > \mathrm{IFC_{bond2}}$$

Through a comparison of IFC among various loops it has been seen that the IFC of the BNB anion in both the EPR-II and EPR-III basis set were all positive. However, in the case of the radical a few nitrogen atoms had negative value.

Therefore, the notable point is that while BNB undergoes changes among its radical anion and cation form, the level of ΔV variation among each bond would be appeared. The ΔV of the first level was less than 100 a.u. which was corresponded to the anionic form, the ΔV of second level was 100–1000 a.u. and referred to the cationic form and in the case of radical the ΔV was more than 1000 a.u. These three layers have been also observed for other performed calculations. Hence, it is evident that our system in different anionic, radical, and cationic forms would involve three states that indicate and confirm the quantized ring rotation. So, it could be imagined that through coupling various macromolecules with rotation axis, i.e., BNB the electron transition will causes the quantized rotation of considered molecules.

The electrical potential of radical anionic and cationic forms of BNB in BNB–$B_{15}N_{15}$ system which have been given in Tables 5 and 6 were all negative and the values fall in two categories. These quantities for B and N atoms were −11 and −18, respectively. It was interesting that in the case of BNB cation the trend of the average of electrical potential variation in each loop was well in accordance with bonds.

Another critical point is that the most negative value of the average electrical potential was corresponded to the

BNB anion (−15) which seems to supports the higher structural stability of BNB anion in compared with radical and cationic states.

The next important quantity was the atomic spin density that has been reported in these tables. First, it should be remembered that no spin density was available for the cationic form of BNB. In the case of the BNB anion all atomic spin densities of B and N atoms involved in each bond and loop were positive. The higher positive values of spin densities of either loops or bonds mainly corresponded to B atoms.

Therefore, based on the results of this section, the non-bonded interaction between the BNB molecule and $B_{15}N_{15}$ ring is dependent on the IFC, the bonding voltage differences (ΔV), the atomic spin density, electrical potential of radical anionic and cationic forms of BNB, and partial atomic charges derived by chelp G calculations.

All the results obtained demonstrated that despite the structural stability of the $B_{15}N_{15}$ ring, it was so sensitive to the presence of the BNB molecule inside the ring and is under the influence of its induced electrostatic field. The structural properties of the $B_{15}N_{15}$ ring had the capability of transferring charges and electromagnetic current to bonds and the charge transfer along the ring and transfer a regular electromagnetic current around the $B_{15}N_{15}$ ring. That is why in the case of the BNB anion the system dipole moment and ΔV values remained constant at all rotational angles. Of course, for the BNB cation and radical cases different quantized values of dipole moments and ΔV values have been observed. Consequently, because of quantized variation of these parameters of energy for the system would also be changed. So, within energy changes, quantities of the system can be exited to higher levels and when it turns back to its ground state the spectrum of quantized parameters would be appeared.

These systems can be used as a Molecularmotor in biomolecular systems. In other words, these molecules can be attached to some sensitive and active site parts of biomolecules and then because of different quantitative voltages, the rotational movements will be appeared and the spectrums of these rotational movements will be calculated.

Conclusion

Due to the chemical importance of electrostatic non-bonded interaction among various nano-systems, the application of DFT methods with EPR basis sets provides a deeper insight into their molecular and hyperfine spectroscopic properties.

In this study, the results of hybrid DFT with EPR quantum-chemical calculations were useful for description of the electromagnetic non-bonded interaction between the $B_{15}N_{15}$ ring and to structural modifications of the radical, cationic, and anionic forms of the BNB molecule.

Because of the electrostatic and hyperfine characteristics of the BH_2NBH_2–$B_{15}N_{15}$ system, those properties dealing with electron distributions around nuclei including relative energies, HOMO–LUMO band gaps, NBO analysis total atomic charges, spin densities, electric potential, and isotropic Fermi coupling constants, and NQR parameters of cationic and anionic forms of BNB in different loops and bonds have been employed to detect and characterize the hyperfine structural properties of the $B_{15}N_{15}$–BNB system.

BSSE and NBO analyses of complexes indicated that the variation of charge densities and the extent of charge transfers correlate well with the interaction energies obtained. The information inferred from the NQR study on local electron density distribution with analysis of atomic charges by the density functional DFT methods, provided appropriate means for determination of reactive atoms and hence, could indicate possible promising directions to be followed in investigation of hyperfine structural properties of nano-systems.

The results obtained revealed the structural stability of the BNB–$B_{15}N_{15}$ system and are proper for investigation of electromagnetic properties of biological systems. So, we could couple the adenine–thymine base pairs with the BNB molecule inside the $B_{15}N_{15}$ ring and repeat the calculations for the three different radical, anionic, and cationic forms of BNB. Based on $\Delta E = h\Delta v$ and replacing each expectation values of relative energies ($\Delta E_{\text{radical–cation}}$, $\Delta E_{\text{radical–anion}}$, and $\Delta E_{\text{anion–cation}}$) three quantized rotational frequencies for $B_{15}N_{15}$–adenine–BHNBH–thymine have been obtained as $v_{\text{radical–cation}} = 31$ THz, $v_{\text{anion–cation}} = 1$ THz, and $v_{\text{radical–anion}} = 29$ THz. However, in the case of $B_{15}N_{15}$–BH_2NBH_2 system the three frequencies were $v_{\text{radical–cation}} = 136$ THz, $v_{\text{anion–cation}} = 179$ THz, and $v_{\text{radical–anion}} = 43$ THz. Considering the range of 1–430 THz as the IR region of the rotational spectrum, it can be seen that all observed frequencies appeared in this region.

It is notable that for each case specific values of dipole moment (the radial component) and ΔV values were obtained and all these values satisfied with Gaussian distributions and different expectation values can be referred to each level. The $B_{15}N_{15}$ ring was so sensitive to the existence of the BNB molecule inside the ring and is under the influence of its induced electrostatic field and the structural properties of this $B_{15}N_{15}$ ring had the capability of transferring charges and electromagnetic current to bonds and the charge transfer along the ring generated a regular electromagnetic current around the $B_{15}N_{15}$ ring. To justify the structural stability of various BNB–$B_{15}N_{15}$ systems, the HOMO–LUMO band gap as the differences between HOMO and LUMO has been found to be a measure of the structural stability and semi-conducting properties of the system.

The interactions caused by electron delocalization have been analyzed by NBO analysis based on the number of natural bonding and anti-bonding orbitals. Also, the coefficients of s and p orbitals of both B–N and B–B bonds involved in radical, cation, and anion $B_{15}N_{15}$–BNB as well as the hybridization of B and N atoms was evaluated based on these NBO data.

The constant coefficients of s and p molecular orbitals of both B–N and B–B bonds involved in radical, cation and anion $B_{15}N_{15}$–BNB which have been extracted from NBO analysis (0.4 and 0.9) inferred to the bonding voltage differences of various B–N bonds and in the case of BNB anion the closeness of the ΔV values (20.642–21.758 a.u.) derived by EPR calculations to the estimation of the sp^2 hybridization of B atom derived by NBO analysis.

Another major point of this study has been focused on the specific usage of $B_{15}N_{15}$–BNB system as a detector for biological molecules which has a possibility of detection of the quantized parameters of a given bimolecular system, which is coupled with this system. In other word, there is mutual electrostatic interaction between BNB and the $B_{15}N_{15}$ ring which cause the quantization of the radial component (r) of the dipole moment vector as well as the voltage differences (ΔV) and relative energies (ΔE) of BNB radical, cation, and anion. The BNB molecule rotates among quantized rotational levels of the radial component (r) of the dipole moment as well as the energy levels. Hence, as a consequence of transitions among quantized levels with given coupled biomolecules the unique spectrum of quantized parameters is distinguishable and this system can act like a biological nano spectrophotometer. These quantized values exhibited a Gaussian distribution and different expectation values could be referred to each quantized level. It seems that investigation of such a non-bonded interaction in the BN cage would be a promising way to improve the physical and chemical properties of fullerenes and may serve as a starting point for designing and considering electromagnetic nano-systems in experiments.

Acknowledgment The portion of this study done in Austin has been supported by grant F-100 from the Welch Foundation.

References

1. Silberberg MS (2009) Chemistry, 5th edn. McGraw-Hill, New York, p 483
2. Crane T, Cowan PBP (2000) Phys Rev B 62:11359
3. Zedlitz R (1996) J Non-Cryst Solids 198–200:403
4. Henager CH Jr (1993) Appl Opt 32:91
5. Weissmantel S (1999) Diam Relat Mater 8:377
6. Leichtfried G (2002) Landolt–Börnstein—Group VIII advanced materials and technologies: powder metallurgy data. Refractory, hard and intermetallic materials. 2A2. Springer, Berlin, pp 118–139
7. Delhaes P (2001) Graphite and precursors. CRC Press, Boca Raton ISBN 9056992287
8. Watanabe K, Taniguchi T, Kanda H (2004) Nat Mater 3:404
9. Taniguchi T, Watanabe K, Koizumi S, Sakaguchi I, Sekiguchi T, Yamaoka S (2002) Appl Phys Lett 81:22–4145
10. Locke IW, Darwish AD, Kroto HW, Prassides K, Taylor R, Walton DRM (1994) Chem Phys Lett 225:186
11. Behrman EC, Foehrweiser RK, Myers JR, French BR, Zandler ME (1994) Phys Rev A 49:R1543
12. Kaxiras E, Jackson K, Pederson MR (1994) Chem Phys Lett 225:448
13. Barone V (1996) In: Chong DP (ed) Recent advances in density functional methods, Part I. World Scientific Publ. Co., Singapore
14. Oku K, Nishiwaki A, Narita I, Gonda M (2003) Chem Phys Lett 380:620–623
15. Slanina Z, Sun M-L, Lee SL (1997) NanoStruct Mater 8(5):623
16. Fowler PW, Rogers KM, Seifert G, Terrones M, Terrones H (1999) Chem Phys Lett 299:359–367
17. Liu Y, Wenli Z, Isaac BB, Boggs JE (2009) J Chem Phys 30:184305
18. Loiseau A, Willaime F, Demoncy N, Schramchenko N, Hug G (1998) Carbon 36(5–6):743-752, 1598
19. Sun ML, Slanina Z, Lee SL (1995) Chem Phys Lett 233:279–283
20. Seifert G, Fowler RW, Mitchell D, Porezag D, Frauenheim T (1997) Chem Phys Lett 268:352–358
21. Takeo O, Masaki K, Hidehiko K, Ichihito N (2001) Int J Inorg Mater 3:597–612
22. Xu SH, Zhang MY, Zhao YY, Cheng BG, Zhang J, Sun CC (2006) Chem Phys Lett 418:297–301
23. Strout DL (2000) J Phys Chem A 104:3364–3366
24. Strout DL (2001) J Phys Chem A 105:261–263
25. Strout DL (2004) Chem Phys Lett 383:95–98
26. Alexandre SS, Mazzoni MSC, Chacham H (1999) Appl Phys Lett 75:61–63
27. Alexandre SS, Nunes RW, Chacham H (2002) Phys Rev B 66:085–406
28. Wu HS, Jiao HJ (2004) Chem Phys Lett 386:369–372
29. Wu HS, Xu XH, Strout DL, Jiao HJ (2005) J Mol Model 12:1–8
30. Rogers KW, Fowler PW, Seifert G (2000) Chem Phys Lett 332:43–50
31. Zhu HY, Schmalz TG, Klein DJ (1997) Int J Quant Chem 63:393–401
32. Manolopoulos DE, Fowler PW (1991) Chem Phys Lett 187: 1–7
33. Zope RR, Dunlap BI (2004) Chem Phys Lett 386:403–407
34. Knight LB Jr, Hill DW, Kirk TJ, Arrington CA (1992) J Phys Chem 96:555
35. Slanina Z, Martin JML, Franqois J-P, Gijbels R (1993) Chem Phys Lett 201:54
36. Slanina Z, Martin JML, Franqois JP, Gijbels R (1993) Chem Phys 178:77
37. Martin JML, Slanina Z, Franqois JP, Gijbels R (1994) Mol Phys 82:155
38. Iijima S, Ichihashi T (1993) Nature 363:603
39. Ajayan PM (1999) Chem Rev 99:1787
40. Maciel GS, Edgardo G (2005) Chem Phys Lett 409:29–33
41. Bayly CI, Cieplak P, Cornell W, Kollman PA (1993) J Phys Chem 97:10269
42. Martin F, Zipse H (2004) J Comput Chem 26:97
43. Chipot C, Maigret B, Rivail J-L, Sheraga HA (1992) J Phys Chem 96:10276
44. Besler BH, Merz KM Jr, Kollman PA (1990) J Comput Chem 11:431
45. Cohen MH, Reif F (1975) Solid State Phys 5:321
46. Lucken EAC (1969) Nuclear quadrupole coupling constant. Academic Press, London

47. Shukla MK, Mishra SK, Kumar A, Mishra PC (2000) J Comp Chem 21:826–846
48. Bors W, Michel C, Stettmaier K, Kazazic SP, Klasinc L (2002) Croat Chem Acta 75(4):957–964
49. Tamulis A, Tsifrinovich VI, Tretiak S, Berman GP, Allara DL (2007) Chem Phys Lett 436:144–149
50. Reed AE, Curtiss LA, Weinhold F (1988) Chem Rev 88:899–926
51. Weinhold F, Landis CR (2001) Chem Educ Res Pract Eur 2:91–104
52. Weinhold F (1998) Natural bond orbital methods. In: Schleyer PvR, Allinger NL, Clark T, Gasteiger J, Kollman PA (eds) Encyclopedia of computational chemistry. Wiley, Chichester
53. Weinhold F (2001) NBO 5.0 Program manual. Theoretical Chemistry Institute and Department of Chemistry, University of Wisconsin, Madison, p 53706
54. Becke AD (1993) J Chem Phys 98:5648
55. Lee C, Yang W, Parr RG (1998) Phys Rev B 37:785
56. Frisch MJ, Trucks GW, Schlegel HB, Scuseria GE, Robb MA, Cheeseman JR, Zakrzewski VG, Montgomery JA Jr, Stratmann RE, Burant JC, Dapprich Ś, Millam JM, Daniels AD, Kudin KN, Strain MC, Farkas O, Tomasi J, Barone V, Cossi M, Cammi R, Mennucci B, Pomelli C, Adamo C, Clifford S, Ochterski J, Petersson GA, Ayala PY, Cui Q, Morokuma K, Malick DK, Rabuck AD, Raghavachari K, Raghavachari JB, Cioslowski J, Ortiz JV, Baboul AG, Stefanov BB, Liu G, Liashenko A, Piskorz P, Komaromi I, Gomperts R, Martin RL, Fox DJ, Keith T, Al-Laham MA, Peng CY, Nanayakkara A, Gonzalez C, Challacombe M, Gill PMW, Johnson B, Chen W, Wong MW, Andres JL, Gonzalez C, Head-Gordon M, Replogle ES, Pople JA (1998) Gaussian 98 Revision A.7. Gaussian, Inc., Pittsburgh
57. Zhang RB, Huyskensd TZ, Ceulemeans A, Nguyen MT (2005) Chem Phys 316:35–44
58. Mayer LI (1998) Chem Phys Lett 297:365–373
59. Jansen HB, Ross P (1969) Chem Phys Lett 3:140
60. Boys SF, Bernar F (1970) Mol Phys 19:553
61. Jenson F (2007) Introduction computational chemistry, 2nd edn. Wiley, New York
62. Culot F, Lievin J (1992) Phys Scr 46:502–517
63. Wrzalik R, Merkell K, Kocot A (2003) J Mol Model 9:248–258
64. Breneman CM, Wiberg KB (1990) J Comput Chem 11:361–373
65. Goodman L, Pophristic V, Weinhold F (1999) Acc Chem Res 32:983–993
66. Reed AE, Weinhold F (1985) J Am Chem Soc 107:1919–1921
67. Myers WK, Scholes CP, Tierney DL (2009) J Am Chem Soc 131(30):10421
68. Latajka Z, Bouteiller Y (1994) J Chem Phys 101:9793–9799
69. Kim K, Jordan KDJ (1994) Phys Chem 98:10089–10094
70. Jalbout AF (2002) Acta Chim Slov 49:643–648
71. Emanuele E, Negri F, Orlandi G (2007) Inorg Chim Acta 360:1052–1062
72. Takahashi O, Yamasaki K, Kohno Y, Ohtaki R, Ueda K, Suezawa H, Umezawa Y, Nishio M (2007) Carbohydrate Research 342:1202–1209
73. Zhang S, Yang P (2005) J Mol Struct: Theochem 757:77–86
74. Kolandaivel P, Nirmala V (2004) J Mol Struct 694:33–38
75. Glendening ED, Faust R, Streitwieser A, Vollhardt KPC, Weinhold F (1993) J Am Chem Soc 115:10952–10957
76. Bruschi M, Giuffreda MG, Lüthi HP (2002) Chem Eur J 8:4216–4227
77. Giuffreda MG, Bruschi M, Lüthi HP (2004) Chem Eur J 10:5671–5680
78. Kjaergaard HG, Henry BR (1994) Mol Phys 83:1099–1116
79. Rosmusb P, Vladimir G, Tyutere V (2000) Chem Phys Lett 331(2–4):317–322
80. Fan J-F, Wang Q, Qi-Ying XIAO, Graaf V (2002) Chin J Struct Chem 21(2):139–141